Journal of
Composites Science

MDPI

Article

Assessment of Web Crippling Capacity of Pultruded GFRP Hollow Profiles Under Various Loading Conditions After Elevated Temperatures

Mohamed Ahmed Soumbourou [1], Ceyhun Aksoylu [2], Emrah Madenci [1,3] and Yasin Onuralp Özkılıç [1,4,*]

[1] Department of Civil Engineering, Necmettin Erbakan University, 42090 Konya, Türkiye
[2] Department of Civil Engineering, Konya Technical University, 42250 Konya, Türkiye
[3] Department of Technical Sciences, Western Caspian University, Baku 1001, Azerbaijan
[4] Department of Unique Buildings and Constructions Engineering, Don State Technical University, Gagarin Sq. 1, 344003 Rostov-on-Don, Russia
* Correspondence: yozkilic@erbakan.edu.tr; Tel.: +90-506-263-98-08

Abstract

This study investigates the residual web crippling behavior of pultruded glass fiber-reinforced polymer (P-GFRP) hollow sections after exposure to elevated temperatures. The primary objective is to evaluate the combined influence of temperature and loading configuration on web crippling capacity, failure mechanisms, and structural performance, and to develop practical prediction models for engineering applications. A total of twenty pultruded GFRP hollow section specimens were exposed to temperatures of 24 °C, 200 °C, 250 °C, 300 °C, and 350 °C and tested under four loading configurations: End Ground (EG), Interior Ground (IG), End Two Flange (ETF), and Interior Two Flange (ITF). In addition to web crippling tests, tensile, SEM-EDS, TGA-DSC, DMA, and FT-IR analyses were conducted to investigate the mechanical, thermal, and microstructural degradation mechanisms. The results showed that elevated temperatures significantly reduced the web crippling capacity, with strength losses reaching up to 80% at 350 °C due to matrix degradation, fiber–matrix debonding, and loss of structural integrity. Among the investigated loading configurations, IG exhibited the highest load-carrying performance, whereas ETF experienced the greatest capacity reduction. A temperature-dependent reduction factor and unified empirical prediction equations were developed and demonstrated good agreement with the experimental results, with experimental-to-predicted ratios ranging from 0.97 to 1.15. The findings provide valuable insight into the post-fire behavior of pultruded GFRP hollow sections and offer practical guidance for the design, assessment, and fire safety evaluation of GFRP structural members exposed to elevated-temperature environments.

Keywords: pultruded GFRP; web crippling; elevated temperature; reduction factor; load-carrying capacity prediction; thermal degradation; fiber–matrix debonding; composite structural design

Check for updates

Academic Editors: Nathália B. D. Lima, Nathan Bezerra De Lima and Kleber G. B. Alves

Received: 23 May 2026
Revised: 16 June 2026
Accepted: 17 June 2026
Published: 19 June 2026

Copyright: © 2026 by the authors. Licensee MDPI, Basel, Switzerland. This article is an open access article distributed under the terms and conditions of the Creative Commons Attribution (CC BY) license.

1. Introduction

Pultruded glass fiber-reinforced polymer (GFRP) is a material that offers the advantages of lightness, excellent corrosion resistance, and high mechanical strength [1,2]. Unlike materials such as reinforced concrete, which is the most common material used worldwide, the main difference lies in the weight of the GFRP and its excellent mechanical properties, such as tensile strength, which could attract the attention of many construction specialists

and prompt recommendations for these uses. Although it is not the most widely used material, it is used in many sectors, such as bridge construction, cooling towers, marine construction, etc., due to the advantages it offers [3–10]. However, like any other material, pultruded GFRP faces a problem that can be considered a disadvantage. This material has stronger mechanical characteristics in the longitudinal direction than in the transverse direction, which is why it is called an anisotropic material. When subjected to transverse loads, pultruded GFRP exhibits failures similar to those identified in steel profiles, namely, web crippling. In the web crippling phenomenon, failure occurs when a concentrated force is applied to a pultruded GFRP profile and the latter does not respond with a sufficient mechanical resistance to the transverse load applied, thus producing various cracks at the intersection of the flange and web, at mid-height of the web, and along the entire web length of the profile (depending on the load application position) [11–15].

This study has become one of the most modern topics, attracting the attention of researchers. But despite all this research, there are still many gaps and complexities. Indeed, it is a completely different subject from other structures such as reinforced concrete, steel structures, etc., which already have advanced design standards and failure analyses such as EUROCODE and others, depending on the country. However, pultruded GFRP composites still have gaps in comprehensive design recommendations due to the complexity of the failure mechanisms and limited experimental work. Many authors have referred to the designed formulas used for thin-walled metallic sections as references because of their characteristics, which are somewhat similar to those of steel structures [16–19].

Many of the effects responsible for the phenomenon of web crippling have been studied in the literature on the different sections of pultruded GFRP profiles, many of which have been included in the effects of different loading conditions, the geometric effects of profiles with and without openings, bearing plates, and a few studies on the effects of temperature [20–24].

The loading conditions most commonly applied by researchers to the specimens are transverse loads, such as EG, IG, ETF, and ITF (Figure 1) [25]. End-ground (EG) is a loading condition in which the transverse load is applied through a bearing plate at the end (top), and the specimen is seated on the ground (a metal piece whose surface is evenly distributed over that of the specimen). Interior-ground (IG) is a type of loading similar to EG, except that the transverse load is applied from the inside through the bearing plate, and the specimen sits on the ground. End-two-flange (ETF) is a loading condition where the transverse load is applied from two bearing plates (top and bottom) at the end. Interior-two-flange refers to transverse loading applied by two bearing plates on the interior side. Some researchers have even mentioned other loadings such as End-one-flange (EOF) and Interior-one-flange (IOF), which correspond to three-point bending tests, but these are rarely used.

The initial study on the effects of bearing length and loading conditions on the web crippling behavior of pultruded GFRP profiles was conducted by Wu and Bai [26]. Four groups of square hollow sections of different dimensions were subjected to loads under ETF, ITF, EG, and IG conditions, with the concentrated loads applied through steel bearing plates of 50 mm in length. A high ultimate load was found when the load was applied from the interior, and the samples were placed on the ground rather than on the support plates. This study clearly shows that pultruded GFRP hollow sections can withstand transverse loads when the samples are placed under IG loading conditions. In addition, the authors specified that transferring the load to a larger effective surface area (internal loading) contributes to an increase in ultimate load. A similar study was reported by [27] with the aim of further investigating the web crippling behavior of pultruded GFRP hollow sections under ETF, ITF, EG, and IG loading conditions. In this study, the authors used different

lengths of support plates to evaluate their effects on web crippling behavior. The lengths of the support plates used were 50 mm, 100 mm, and 150 mm. It was found that increasing the length of the support plates had no impact on the evolution of the ultimate load. Many researchers [28–30] have also reported that openings in pultruded GFRP I-sections and U-channels have a major effect on web crippling behavior. As for temperature effects, studies have reported that the thermophysical characteristics of pultruded GFRP materials deteriorate with increasing temperature, especially with the loss of a significant amount of the matrix phase [31,32]. The web crippling behavior of pultruded GFRP sections at elevated temperatures has been studied by Zhang et al. [16]. A series of pultruded GFRP I-section profiles exposed to temperatures of 20 °C, 100 °C, and 220 °C were subjected to transverse loads under ETF and EG conditions. Excessive reductions in ultimate load were observed under all loading conditions. In addition, a significant reduction in stiffness relative to the ultimate load was also observed.

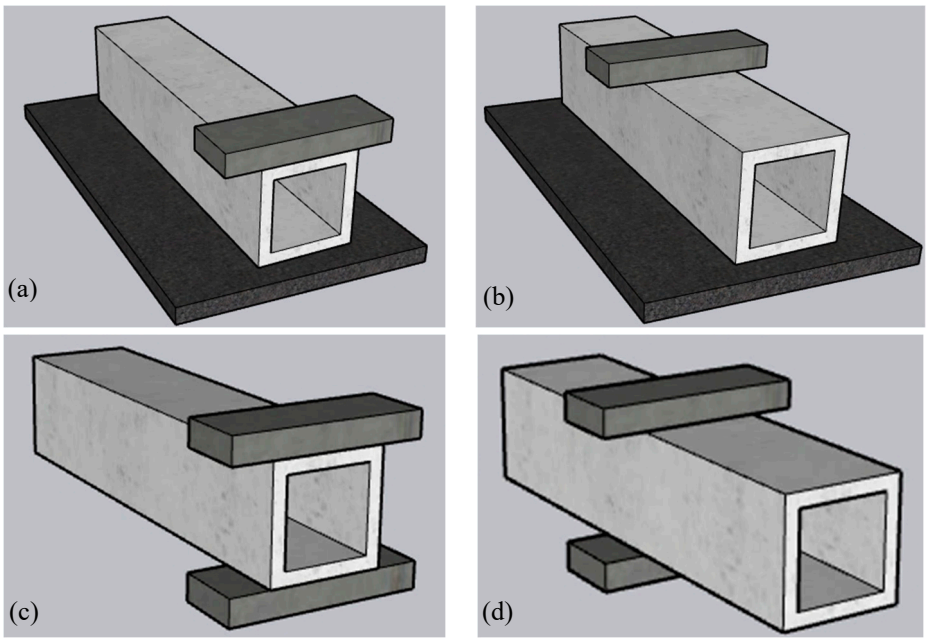


Figure 1. Representation of transversal loading conditions. (**a**) End bearing with solid Ground (EG), (**b**) Interior bearing with solid Ground (IG), (**c**) End-Two Flange (ETF), (**d**) Interior-Two-Flange (ITF).

Although several studies have investigated the web crippling behavior of pultruded GFRP materials under different loading conditions, research addressing the combined effects of elevated temperature and loading configuration on the web crippling capacity of hollow pultruded GFRP sections remains very limited. In particular, there is insufficient information regarding strength degradation mechanisms, failure mode evolution, and reliable capacity prediction models for pultruded GFRP hollow sections subjected to elevated temperatures. Therefore, this study aims to experimentally evaluate the influence of temperature and loading configuration on web crippling behavior and to propose practical reduction factors and prediction equations for engineering applications.

The novelty of this study lies in the comprehensive assessment of the web crippling behavior of pultruded GFRP hollow sections subjected to elevated temperatures under four different loading configurations (EG, IG, ETF, and ITF). Unlike previous studies, which primarily focused on either loading conditions or limited temperature ranges, the present study systematically evaluates the combined influence of temperature and loading configuration on structural performance. Furthermore, a unified prediction approach is proposed by incorporating both temperature-dependent degradation effects and loading

configuration parameters into a single capacity prediction framework. The proposed model provides practical design-oriented equations and reduction factors for estimating the web crippling capacity of pultruded GFRP hollow sections exposed to elevated temperatures.

2. Experimental Study

2.1. Specimens' Preparation

A set of 20 pultruded GFRP hollow sections measuring 100 mm in height and 100 mm wide were cut to lengths of 250 mm using a cutting machine (Figure 2). The size of the specimens was determined based on the ASCE standard [33], which states that the length of the specimen must be more than 1.5 times its height. Once the specimens had been cut to the desired lengths, they were separated into five groups of four specimens to prepare them for the burning test. Four specimens at a room temperature of 24 °C were left unexposed, and the remaining specimens were placed in the oven. The specimens were exposed to temperatures of 200 °C, 250 °C, 300 °C, and 350 °C for 1 h.

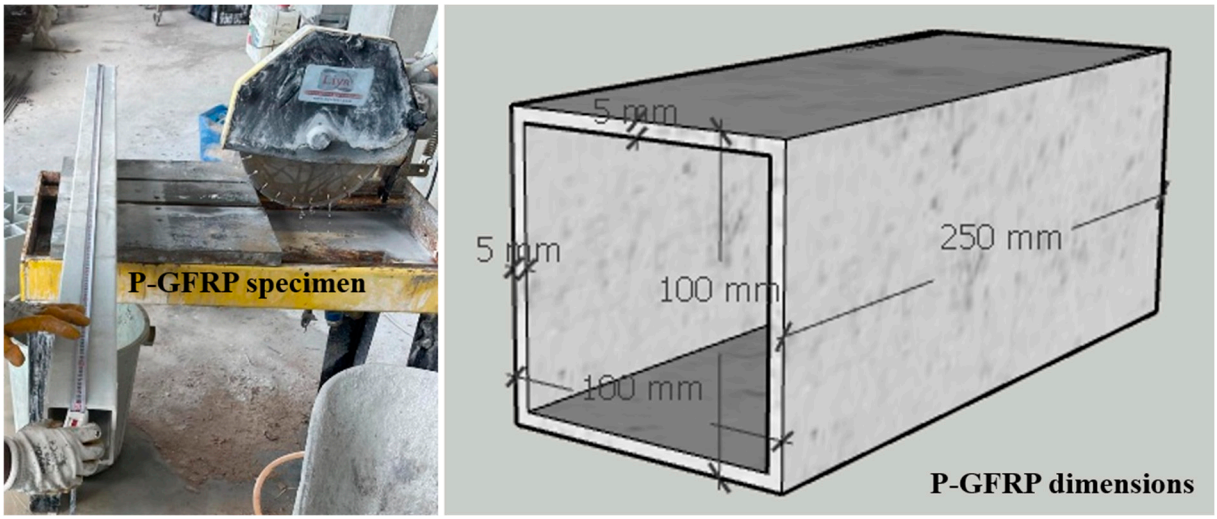


Figure 2. Cutting of the specimens and dimensions of the specimens.

2.2. Test Procedure

The test setup is illustrated in Figure 3. For the loading tests, machines with a maximum load capacity of 600 kN were utilized. Two support plates were used to apply transverse loads. A metal support plate 100 mm wide and 250 mm long was used as a "ground" support on which the sample was seated, and the second support was a metal plate 100 mm wide and 1 mm thick in cases where the load was not applied through the ground. Four loading conditions, including EG, IG, ETF, and ITF (Figure 4), were examined.

The specimens underwent significant changes after being exposed to high temperatures (Figure 5). The first noticeable change in the specimens was a change in color. At 200 °C, the specimens turned yellow; at 250 °C, they turned brown; at 300 °C, they turned brownish–black; and at 350 °C, the material completely blackened (Figure 6). At 350 °C, not only did the specimen burn, but we also noticed that this was the maximum temperature that the specimens could withstand. The material swelled at its surface. The composition of the laminate began to detach (Figure 7). The composition of the fiber and matrix phases became heterogeneous. Even without testing the 350 °C specimens with transverse loads, we could see that the specimens could not withstand loads comparable to those sustained by the specimens exposed to lower temperatures.



Figure 3. Test Set-up.



Figure 4. (**a**) EG, (**b**) ETF, (**c**) ITF, (**d**) IG loading condition.

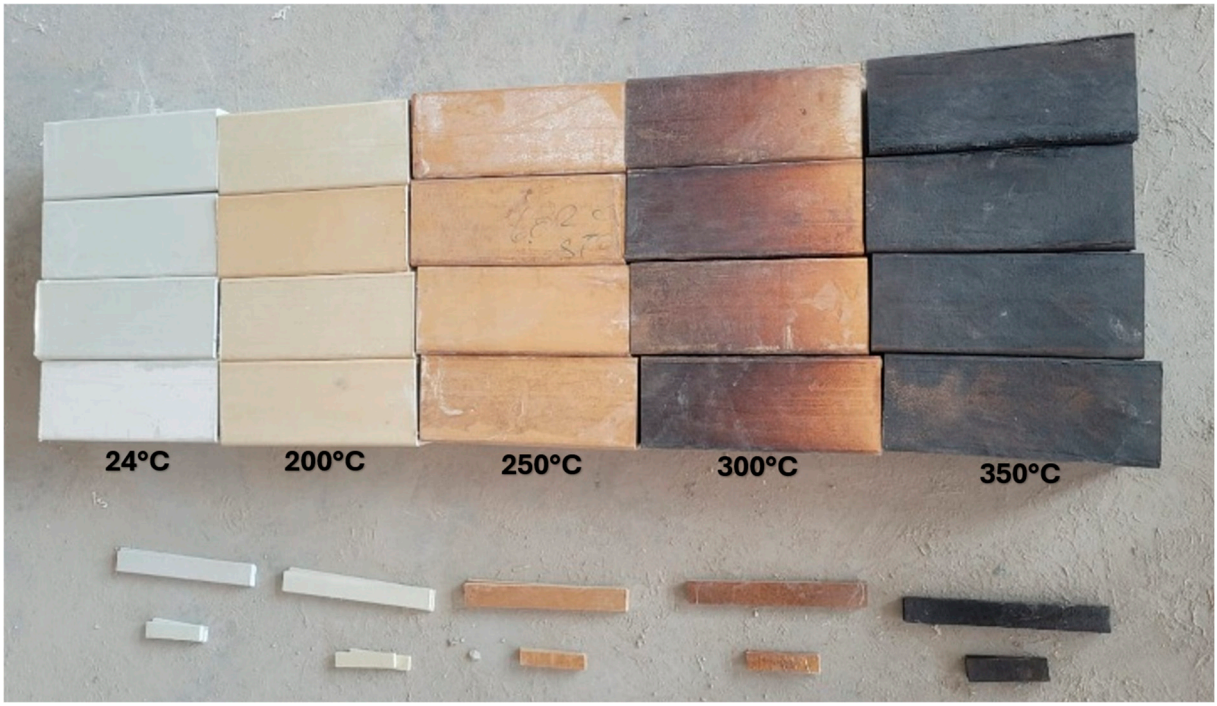


Figure 5. Different P-GFRP hollow sections exposed to different temperatures.

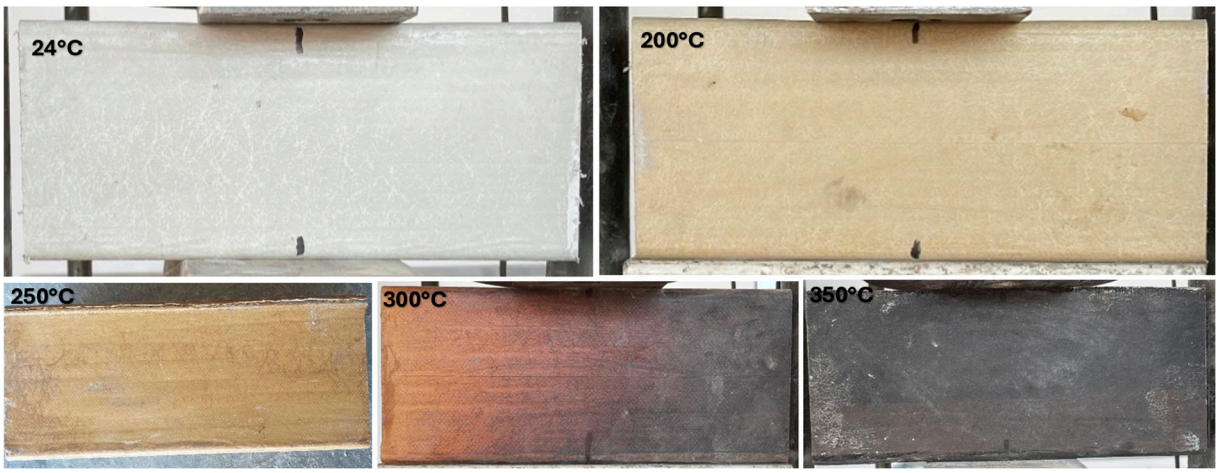


Figure 6. Color changes on the specimens due to temperature.

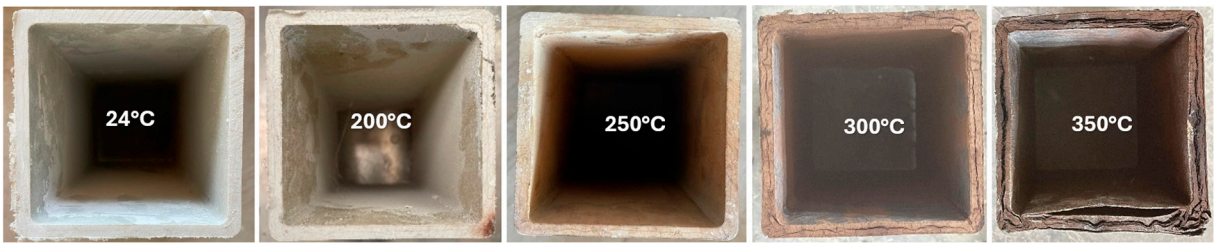


Figure 7. Cross-sectional states with temperature variation.

2.3. Tensile Tests

Tensile tests were conducted to investigate the tensile behavior of GFRP hollow profiles produced by pultrusion after exposure to different temperatures. The tests were conducted on a SHIMADZU AGS-X (100 kN capacity, Kyoto, Japan) universal testing machine located in the Necmettin Erbakan University BİTAM laboratory. Test samples for tensile tests were prepared with a length of 200 mm, a width of 25 mm, and a thickness of 5 mm. Five temperature groups were established: 24 °C (room temperature), 200 °C, 250 °C, 300 °C, and 350 °C. The samples from each temperature group were all held in the oven at the appropriate temperature for one hour and then cooled to room temperature before the tests commenced. Tensile tests were performed at a constant displacement rate of 2 mm/min, and each sample was tested until failure. The stress–strain (σ–ε) curves occurring during the test were recorded.

2.4. Burn-Off Test

A sample of pultruded GFRP hollow section was selected for burn-off testing in order to determine the different components and fiber orientations of the material in accordance with ASTM D2584 [34]. The sample selected was one that had not been subjected to high temperatures but to which a transverse load had already been applied, i.e., a sample that had already been damaged (Figure 8). The initial weight of the sample was measured, and the sample was then placed in an oven at a temperature of 600 °C for one hour. After one hour of heating at 600 °C, the resin component contained in the material had completely evaporated, leaving only the fiber structure (Figure 9). The fiber structure could not withstand the evaporation of the resin component and collapsed completely. In the fiber architecture, it was identified that the manufacturer of the samples used two types of fiber laminates: unidirectional roving glass and continuous stand mat glass. The exterior facades of the sample were composed of continuous stand mat glass, while the interior was more concentrated with unidirectional roving fiber. The composition of unidirectional roving fiber represented a higher percentage (77%) of the fibers, while the multi-directional fiber layer represented 23%. The pultruded GFRP hollow section profile used in the experiment was composed of approximately 66% fiber and 34% resin, according to the burn-off test performed. This reflects a key characteristic of the pultrusion method, which uses a high amount of fiber.



Figure 8. Pultruded GFRP sample before burn-off test.



Figure 9. Pultruded GFRP sample after burn-off test.

2.5. Scanning Electron Microscopy and Energy Dispersive Spectroscopy (SEM-EDS)

Scanning Electron Microscopy (SEM) and Energy Dispersive Spectroscopy (EDS) analyses were performed to investigate the microstructural changes in pultruded GFRP hollow profiles after exposure to elevated temperatures. The aim of these analyses was to observe changes in the matrix decomposition, void formation, and chemical composition at the fiber–matrix interface in samples exposed to different temperatures. Analyses were carried out at the laboratories of Necmettin Erbakan University BİTAM. Separate samples were prepared and analyzed for each temperature level (24 °C, 200 °C, 250 °C, 300 °C, and 350 °C). Sections of appropriate sizes were taken from the samples; their surfaces were smoothed by sanding and cleaned with alcohol. Gold plating (sputter coating) was applied to the surfaces under vacuum to ensure electron conductivity. Imaging was performed in low-vacuum mode using a Hitachi SU 1510 model SEM. The fiber–matrix interfaces, delamination regions, and surface roughness were investigated qualitatively at all magnifications. Additionally, EDS analyses were performed for each temperature condition to evaluate the distribution of chemical constituents found on the surfaces of the samples. The primary purpose of these analyses was to observe the overall changes, such as matrix decomposition, loss of carbon, and an increase in the oxygen content with elevated temperatures.

2.6. Thermogravimetric Analysis (TGA)

Thermogravimetric Analysis (TGA) and Differential Scanning Calorimetry (DSC) tests were carried out to examine the thermal stability and degradation performance of pultruded GFRP hollow profiles under high-temperature conditions. The purpose of these studies was to determine the temperature response, weight loss, and, more importantly, the phase transition temperatures of the matrix and fiber constituents within the composite materials. TGA and DSC tests were conducted using the Setaram–Labsys Evo brand analyzer at the Necmettin Erbakan University BİTAM laboratories. The samples were prepared using a microbalance to weigh approximately 10–15 mg. The tests were carried out from 24 °C to 600 °C in a nitrogen (N_2) atmosphere, with a heating rate of 10 °C/min in both TGA and DSC analyses. The tests were carried out on samples that were exposed to 24 °C (reference) and 350 °C.

2.7. Dynamic Mechanical Analysis (DMA)

Dynamic Mechanical Analysis (DMA) was performed to evaluate the thermomechanical response of pultruded GFRP hollow profiles to temperature changes. Parameters such as glass transition temperature (Tg), storage modulus (E′), loss modulus (E″), and damping

factor (tan δ) were obtained from this analysis. The tests were carried out at a constant frequency of 1 Hz under controlled temperature increase. DMA data obtained from the tests revealed the viscoelastic behavior of the material under the influence of temperature.

2.8. Fourier Transform Infrared Spectroscopy (FT-IR)

Fourier Transform Infrared Spectroscopy (FT-IR) analysis was applied to determine the chemical structural changes in pultruded GFRP hollow profiles under the influence of temperature. This analysis specifically investigated temperature-induced bond breakage, oxidation, pyrolysis initiation, and functional group changes in the epoxy matrix phase. The spectral range of 4000–500 cm^{-1} was selected. The spectra obtained from FT-IR analysis showed the changes that occurred with temperature in the functional groups of the epoxy matrix.

3. Experimental Test Results

3.1. Tensile Test Results

A strong correlation between temperature variation and tensile strength was observed in the specimens. The ultimate load decreased as the temperature of the specimens increased. Furthermore, when the specimens were placed in the tensile testing machine, difficulties were encountered with the placement of the specimens subjected to temperatures of 350 °C. Because the laminates of the latter were slightly detached at high temperatures, the two ends of the specimens fixed in the jaws moved during tensile loading. Therefore, the two surface laminates were removed in order to accurately determine the tensile strength of all specimens. The tensile strengths of the specimens taken in the longitudinal and transverse directions were compared (Figure 10). At all temperatures, the tensile strength was more than ten times higher in the longitudinal direction than in the transverse direction. In addition, the displacement was very significant for the specimens subjected to temperatures of 350 °C in both directions. This severe temperature-dependent anisotropy and the dramatic loss of transverse integrity provided a fundamental phenomenological background for the web crippling behavior. Since the web crippling mechanism is heavily governed by localized transverse compression, matrix cracking, and fiber–matrix debonding, the rapid degradation of the polymer matrix observed in these material-level tests explained the shared root cause behind the structural capacity reduction at elevated temperatures.

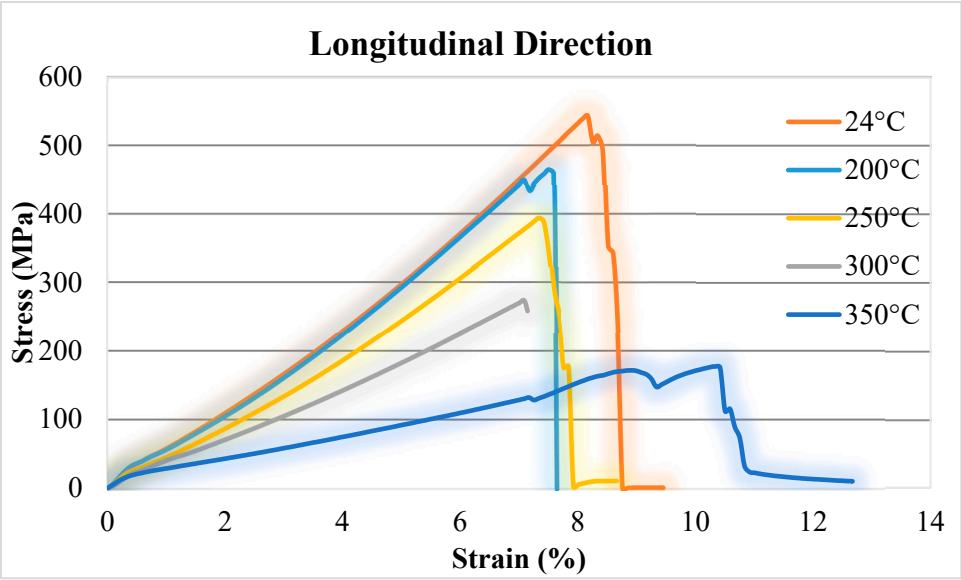


Figure 10. *Cont.*

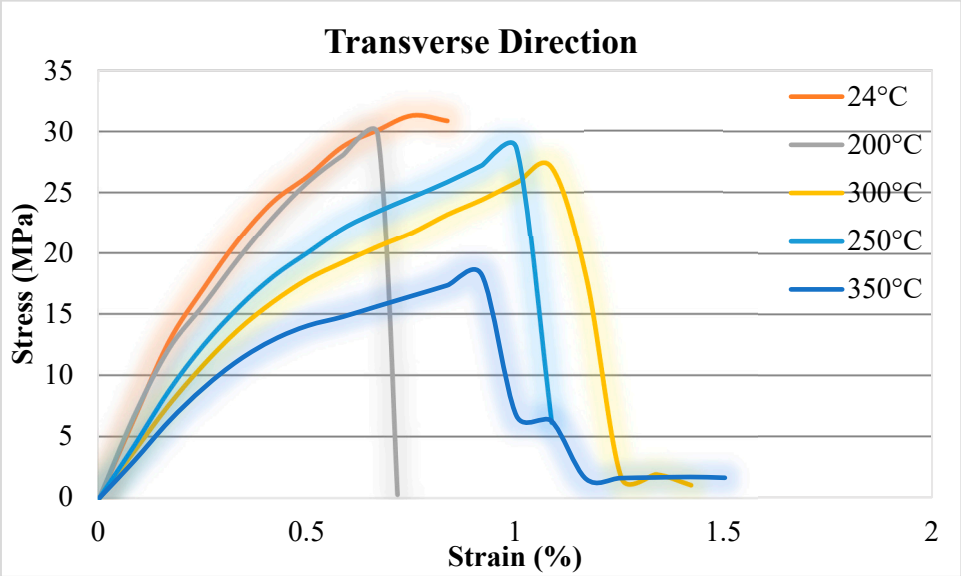


Figure 10. Tensile Test Results.

3.2. Microstructure Analysis Results

3.2.1. SEM+EDS Results

Scanning Electron Microscopy (SEM) and Energy Dispersive X-Ray Spectroscopy (EDS) analyses were performed to investigate microstructural changes in GFRP hollow profiles produced using the pultrusion method under high temperatures. These analyses were used to observe the fiber–matrix interface, the degree of matrix degradation, and changes in surface morphology. Analyses were conducted on samples exposed to temperatures of 24 °C, 200 °C, and 300 °C.

SEM images of samples at 24 °C (room temperature) showed that the glass fibers were bonded cohesively with the epoxy matrix and maintained a homogeneous structure (Figure 11). Matrix penetration down to the fiber core was observed, with no signs of delamination or debonding. This indicates that the composite initially had ideal mechanical performance conditions. The matrix adhered tightly to the fiber surface, and manufacturing errors were minimal. The hard, glassy epoxy phase completely surrounded the fibers before they were exposed to high temperature.

EDS analysis, performed to investigate the chemical composition of pultruded GFRP hollow profiles at room temperature, revealed the basic elemental distribution of the material (Figure 12). The evaluation was carried out within the cross-sectional area exhibiting the glass, fiber, and epoxy matrix phases. The elevated carbon (C) concentration (52.13% by weight) suggests a predominance of the epoxy-based matrix structure, as shown in the example. This ratio is consistent with the typical structural properties of thermoset polymers. Oxygen (O) is the second most dominant element, with a content of 33.51%. This is because both the epoxy structure and the glass fibers contain oxygen-containing groups. The elements silicon (Si) and calcium (Ca) originate from the glass fiber phase. Inorganic oxides such as SiO_2, CaO, and Al_2O_3 are known to be used in glass fiber production. Although the aluminum (Al) element was present in small amounts, it is part of the characteristics of the glass-reinforced structure. These data demonstrate that the GFRP composite tested at room temperature possessed the expected elemental composition and showed no signs of thermal degradation. This analysis will form the basis for assessing the extent of chemical degradation when compared with future temperature analyses.

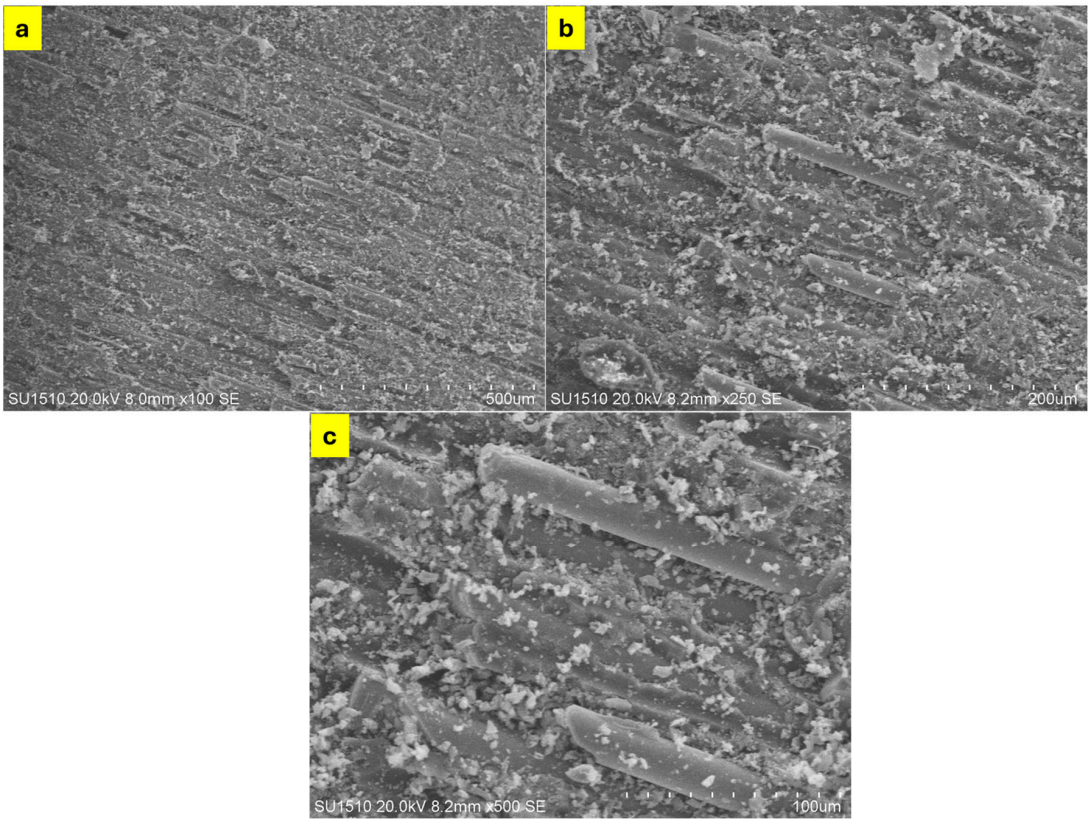


Figure 11. (**a**–**c**) SEM image of samples at 24 °C (room temperature).

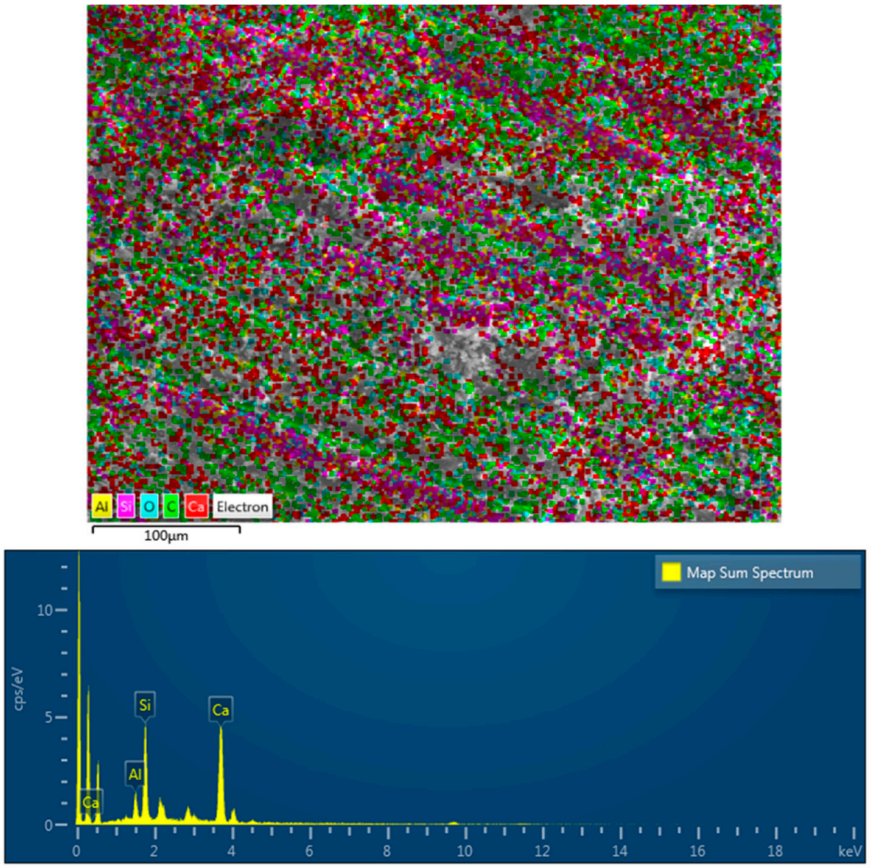


Figure 12. EDS scan image and map of the sum spectrum of samples at 24 °C (room temperature).

At 200 °C, SEM analysis was conducted to determine the effects of high temperature on the matrix–fiber interface (Figure 13). This temperature is close to the glass transition temperature (Tg) of the epoxy matrix, a critical region where visible changes in the microstructural integrity of the structure begin. In Figure 13a, microcracks and matrix separation can be observed around the glass fiber. The matrix's ability to adhere to the fiber surface had begun to weaken, and irregularities had appeared at the fiber–matrix interface. Furthermore, partial fiber separation and void formation are noticeable in some areas. Figure 13b shows more clearly the microscopic voids that formed in the matrix phase. These voids resulted from the epoxy matrix softening under the influence of temperature, which decreased its viscosity and caused it to separate from the fibers. The fibers remained clearly visible, but the beginnings of delamination were observed in some areas. Roughening of the glass fiber surfaces and areas where matrix residues were unevenly distributed were detected in Figure 13c. This indicates that the matrix began to dissolve locally due to thermal effects, and the fiber–matrix bond quality decreased.

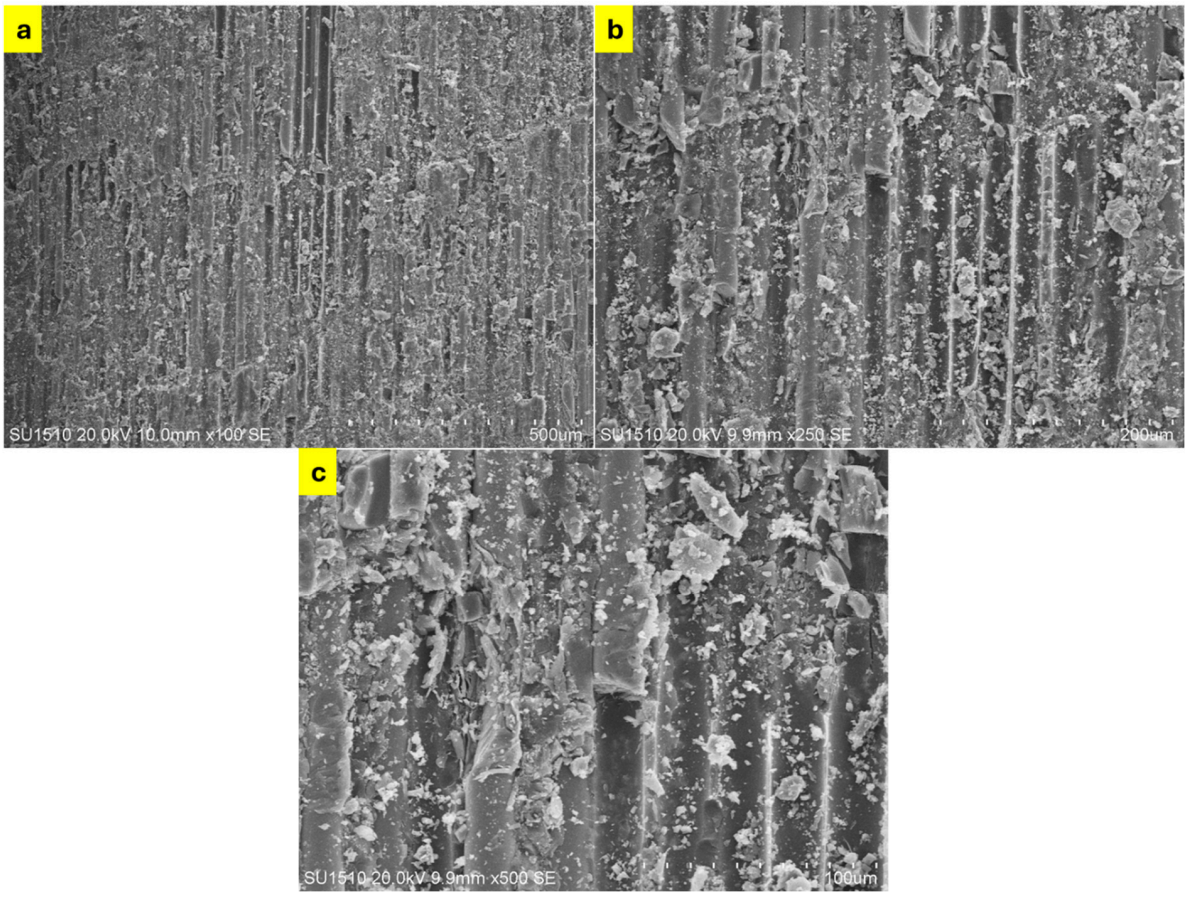


Figure 13. (**a**–**c**) SEM image of the samples at 200 °C.

The EDS analysis results of GFRP hollow profiles exposed to 200 °C are shown in Figure 14. The carbon (C) ratio increased slightly from 52.13% to 55.65% compared to room temperature. The disparity may also stem from the sampling site, as fiber and matrix density may have a localized distribution. The oxygen ratio decreased slightly from 33.51% to 30.87%, correlating with the onset of the decomposition of oxygenated groups. The calcium and silicon ratios remained roughly constant, demonstrating that the glass fiber structure was chemically stable at this temperature. The proportion of aluminum (Al) also decreased from 1.34% to 1.32% and remained almost unchanged. This indicates that the epoxy matrix had not yet undergone large-scale thermal degradation, but microscopic

decomposition had begun, accompanied by a decrease in oxygen content and interface disruption. When evaluated together with the SEM images, it can be concluded that 200 °C had only initial, observable effects on the microstructure.

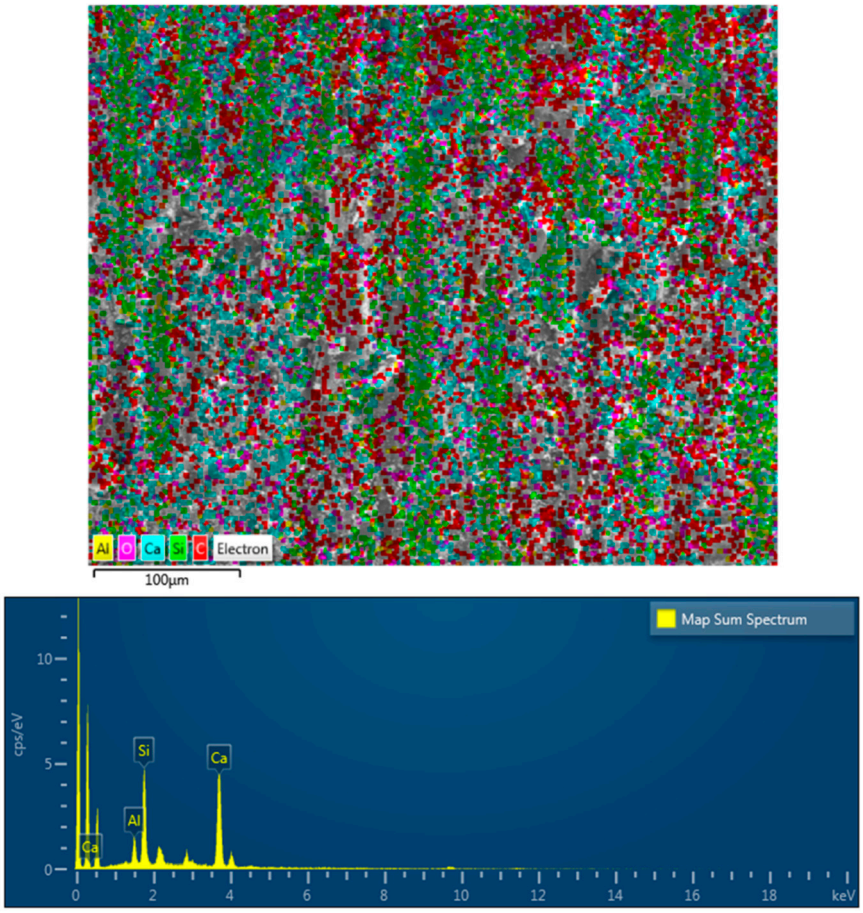


Figure 14. EDS scan image and map of the sum spectrum of samples at 200 °C.

The SEM images obtained after exposure of pultruded GFRP hollow profiles to 300 °C show that the fiber–matrix bonds have been disrupted, and the composite has largely lost its microstructural integrity (Figure 15). The glassy structure of the matrix has weakened, and the adhesion around the fibers has largely disappeared.

In Figure 15a, it is clearly observed that the glass fibers had largely separated from the matrix, and the matrix phase had been pulled apart and fragmented. Significant delamination and fiber clusters are visible at the interface. This indicates that the matrix had lost its mechanical binding properties at temperatures below 300 °C. Figure 15b shows the microscopic voids and pore structure within the matrix. These structures are the result of thermal dissolution of the matrix and the decomposition of volatile components. The matrix residues around the fibers are observed in a scattered and irregular pattern. In Figure 15c, the random distribution of matrix residue on the surface of the glass fibers, with some areas completely exposed, is noteworthy. The inter-fiber bonding structure is virtually eliminated, leaving the structure completely disintegrated This indicates a significant decrease in mechanical strength. A temperature of 300 °C can be considered the critical temperature at which GFRP composite materials lose much of their microstructural integrity. SEM analyses show that the matrix degrades, fibers separate, pores increase, and the surface morphology is severely damaged.

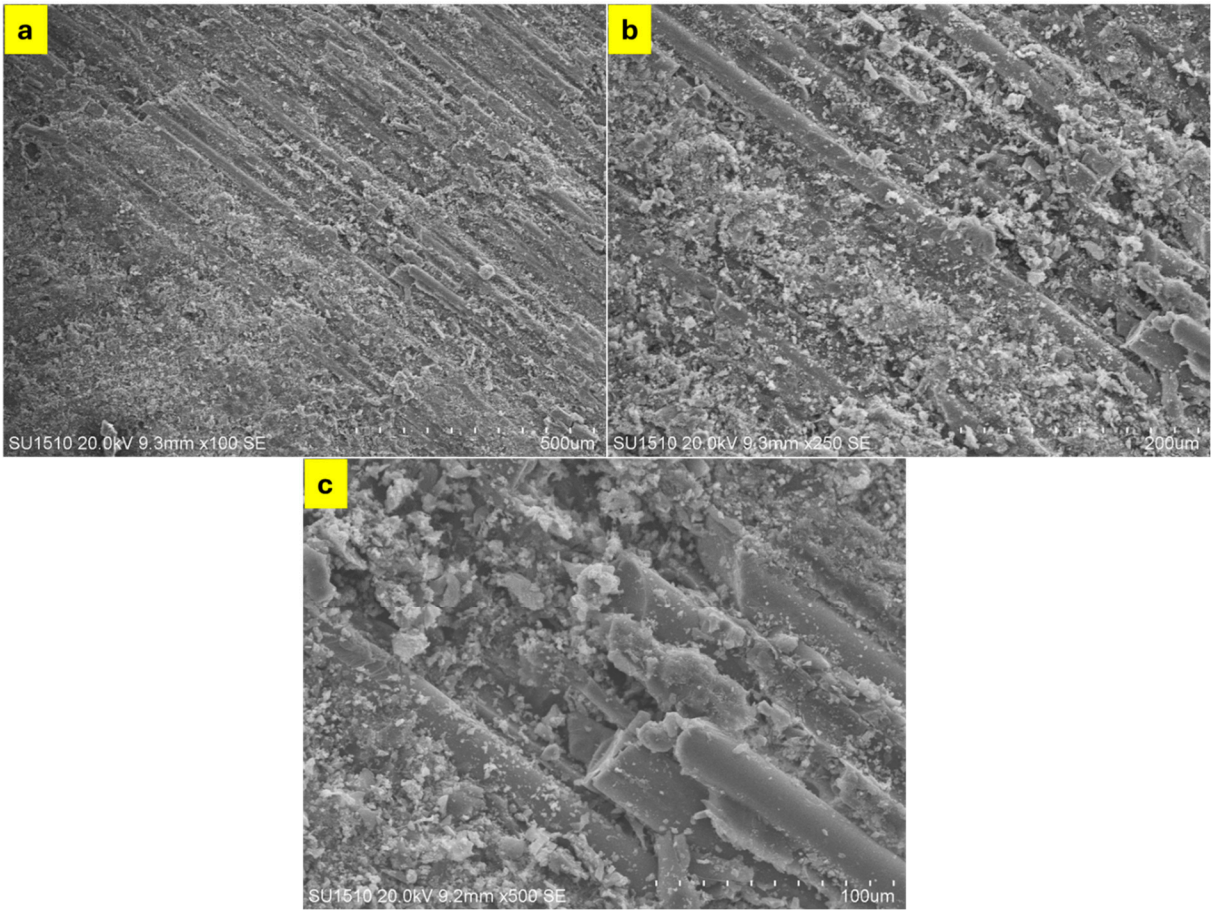


Figure 15. (**a**–**c**) SEM image of the samples at 300 °C.

The EDS analyses performed indicate that at 300 °C, the epoxy matrix begins to lose thermal stability, its carbon content decreases, and oxidative structures form. The glass fiber components (Si, Ca, Al) remained generally stable but became more visible on the surface (Figure 16). The carbon (C) proportion exhibited a negligible decrease from 55.65% to 54.16% compared to 200 °C. Such a decrease implies that the epoxy matrix had begun to undergo progressive thermal degradation and that the carbon-based structure was partially degraded. The oxygen (O) proportion increased by 31.83% compared to 200 °C. This indicates that oxidative reactions occurred under the influence of temperature and that oxygenated groups were released by the degradation of the polymer chains. The silicon (Si) and calcium (Ca) proportions represent the chemical structure of the glass fiber and remain structurally stable components. In contrast, however, Si exhibited a slight increase relative to 200 °C, as evidenced by its exposure in SEM images. The aluminum (Al) content also displayed an increase compared to 200 °C because the alumina phases, which are present within the glass fiber reinforcement, become more prominent.

The elemental composition obtained as a result of EDS analysis of samples from 24 °C to 300 °C is given in Table 1.

Table 1. Elemental composition, weight (%).

Degree	C (%)	O (%)	Si (%)	Ca (%)	Al (%)
24 °C	52.13	33.51	4.40	8.61	1.34
200 °C	55.65	30.87	4.24	7.92	1.32
300 °C	54.16	31.83	4.97	7.44	1.60

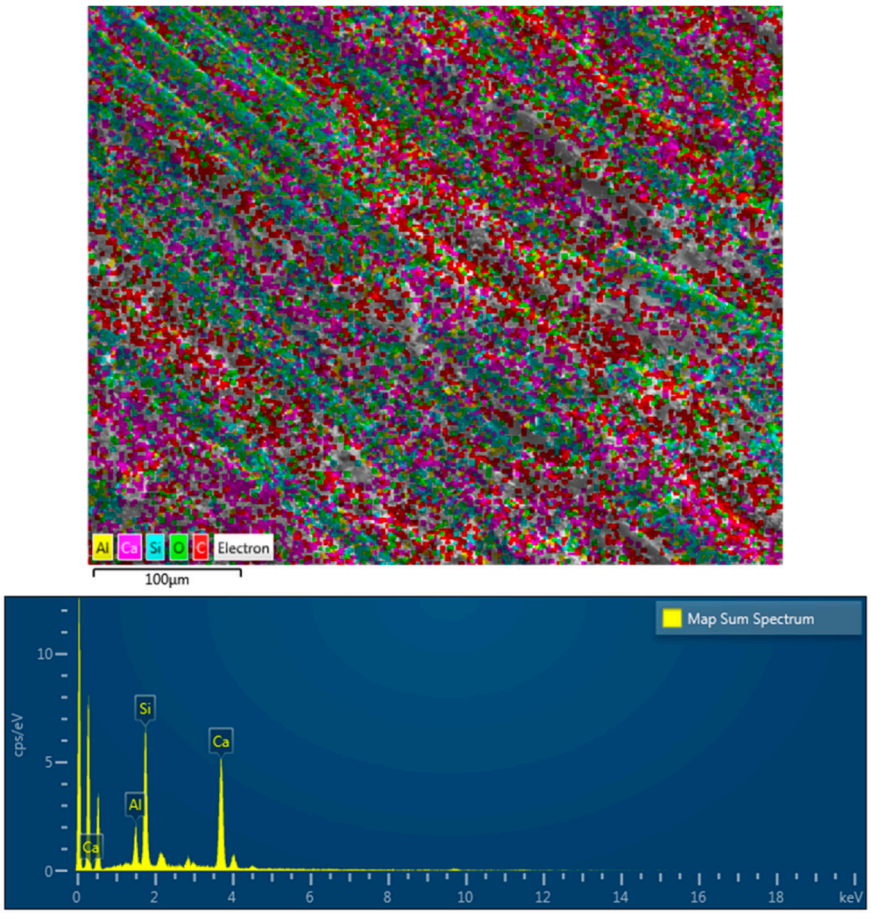


Figure 16. EDS scan image and map of the sum spectrum of samples at 300 °C.

3.2.2. Thermal Analysis Results (TGA–DSC)

TGA (Thermogravimetric Analysis) and DSC (Differential Scanning Calorimetry) tests were performed on samples exposed to temperatures of 24 °C, 300 °C, and 350 °C to determine the thermal behavior of GFRP hollow profiles. Analyses were conducted over a temperature range from 24 °C to 600 °C. The thermal stability and decomposition temperatures were determined from the TGA and DSC curves. The TGA curve for the reference sample stored at room temperature begins with a slow mass loss starting at 25 °C and shows a pronounced decomposition trend at approximately 390 °C (Figure 17). This decomposition represents the temperature at which the epoxy matrix begins to lose its structural integrity. The sudden mass-loss trend observed in the curve between ~390–460 °C corresponds to the pyrolytic decomposition of the thermoset resin.

The sample, preheated to 300 °C, was reheated from 25 to 600 °C in the TGA test (Figure 18). In this sample, the total mass loss remained at 26.21% because some of the matrix had already decomposed. However, the main decomposition process began at 391.28 °C, indicating that the matrix still retained some thermal stability. Thermal effects were more pronounced in the sample pretreated at 350 °C (Figure 19). The onset of degradation was measured at approximately 384.89 °C. This indicates that the matrix had become structurally unstable and began to decompose at a lower temperature. The total mass loss was 26.28%, very similar to that of the 300 °C sample. This decrease indicates that thermal bifurcation and oxidative degradation had begun in the epoxy network structure, thus shifting the degradation threshold downwards.

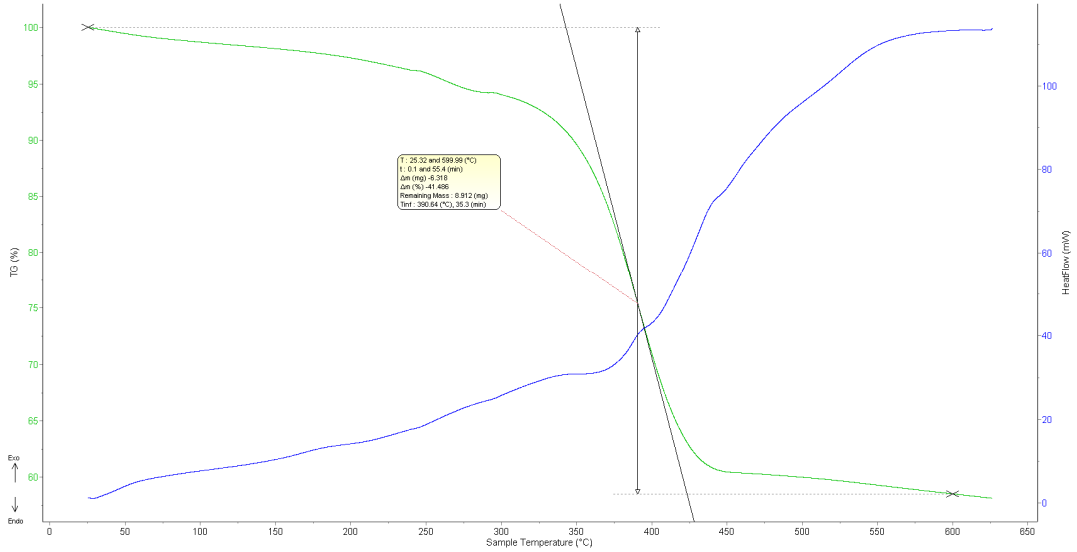


Figure 17. TGA-DSC results of samples tested at room temperature (24 °C).

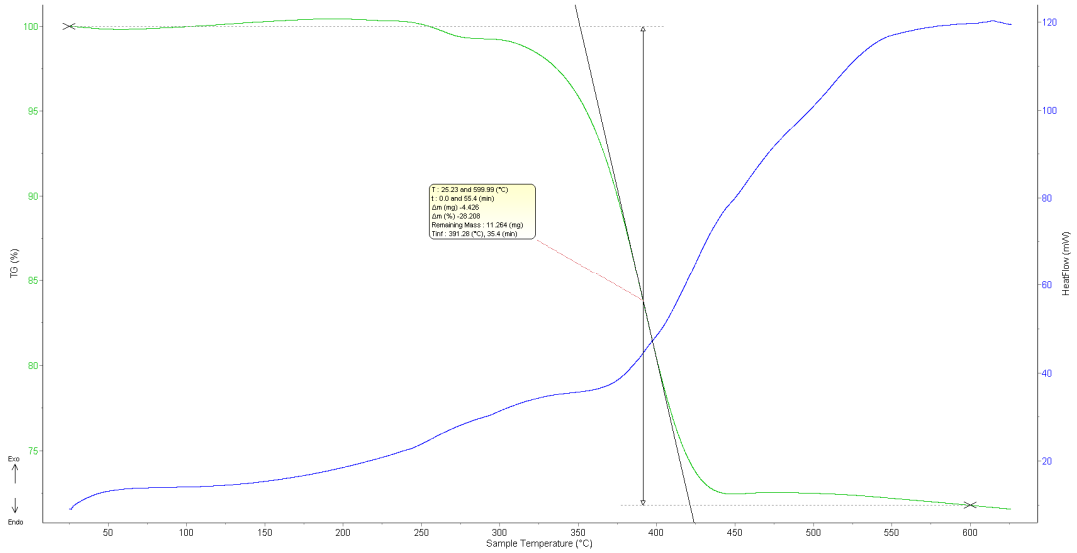


Figure 18. TGA-DSC results of samples tested at 300 °C.

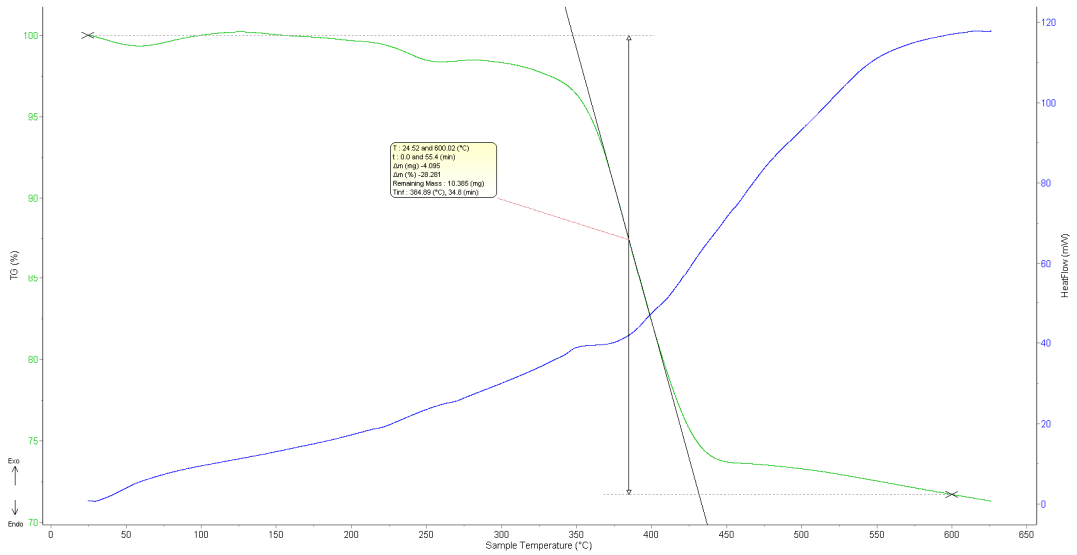


Figure 19. TGA-DSC results of samples tested at 350 °C.

3.2.3. Dynamic Mechanical Analysis (DMA) Results

Dynamic Mechanical Analysis (DMA) was used to analyze the samples' viscoelastic behavior as a function of temperature. This process investigated fundamental mechanical parameters, including storage modulus (stiffness), loss modulus, and damping factor (tan δ) at specific temperature and frequency conditions. DMA provides critical data, particularly for the glass transition temperature (Tg), the temperature range within which elastic behavior is limited, and the monitoring of heat treatment effects.

Looking at Figure 20, the DMA curve of the reference sample shows that the storage modulus initially stands at around 6.1×10^8 Pa but decreases at higher temperatures. This clearly implies that with the rise in temperature, the polymer matrix loses some of its elastic strength. As for the tan δ curve, it starts at a low value of approximately 0.02 and rises sharply with temperature, reaching a maximum at about 139.59 °C.

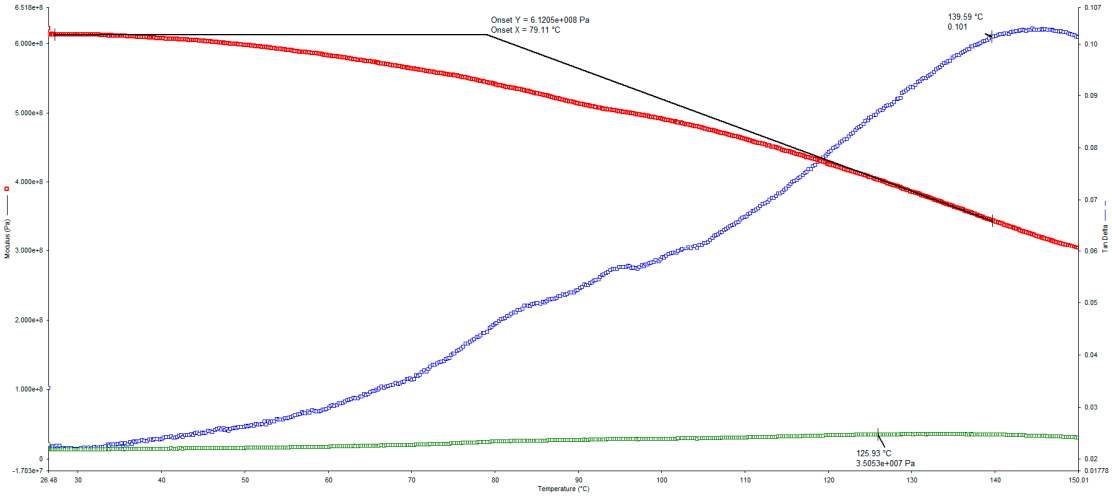


Figure 20. DMA results of samples tested at room temperature (24 °C).

When the sample was subjected to a heat treatment at 200 °C, the modulus values were lower (~3.0×10^8 Pa) than those of the reference sample (Figure 21). This decrease is attributed to polymer chain relaxation at high temperatures, the distribution of the crystalline structure, and the possible formation of microvoids. The tan δ initially exceeded that of the reference sample and then decreased over time. The heat treatment may have introduced amorphous regions into the grain and a slightly softer structure capable of absorbing more energy.

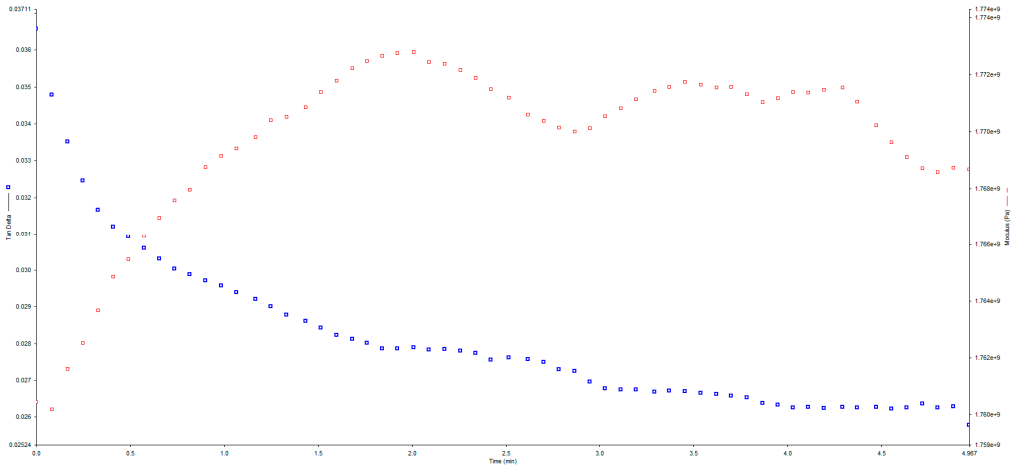


Figure 21. DMA results of samples tested at 200 °C.

With a modulus of around 4.65 × 10^8 Pa, the structure of the sample heated to 250 °C was more rigid than the sample heated to 200 °C (Figure 22). This magnitude of improvement has to do with the rearrangement of polymer chains and the formation of semi-crystalline regions during heat treatment. The lower tan δ value thus indicates that the structure absorbs less energy internally and behaves more like an elastic-type structure. This aligns with the notion that heat treatment at moderate temperatures induces the formation of semi-crystalline microstructures in the material, which, in turn, helps to improve the mechanical behavior.

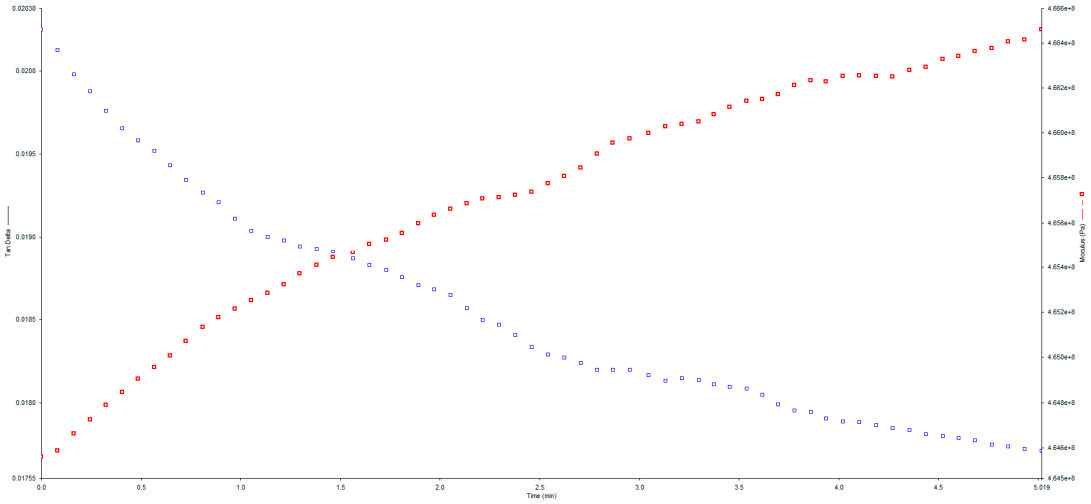


Figure 22. DMA results of samples tested at 250 °C.

The highest value of the modulus was obtained for the sample heat-treated at 300 °C (~1.77 × 10^9 Pa) compared with the other groups (Figure 23). This maximum mechanical strength could be due to either cross-linking or the regular arrangement of the polymer chains. The low magnitude of tan δ and its progressive decrease over the measured time suggest that viscoelastic behavior did not dominate; rather, elastic (rigid) behavior occurred. These results indicate that heat treatment at 300 °C highly stabilizede the polymer structure, increasing hardness and reducing energy dissipation.

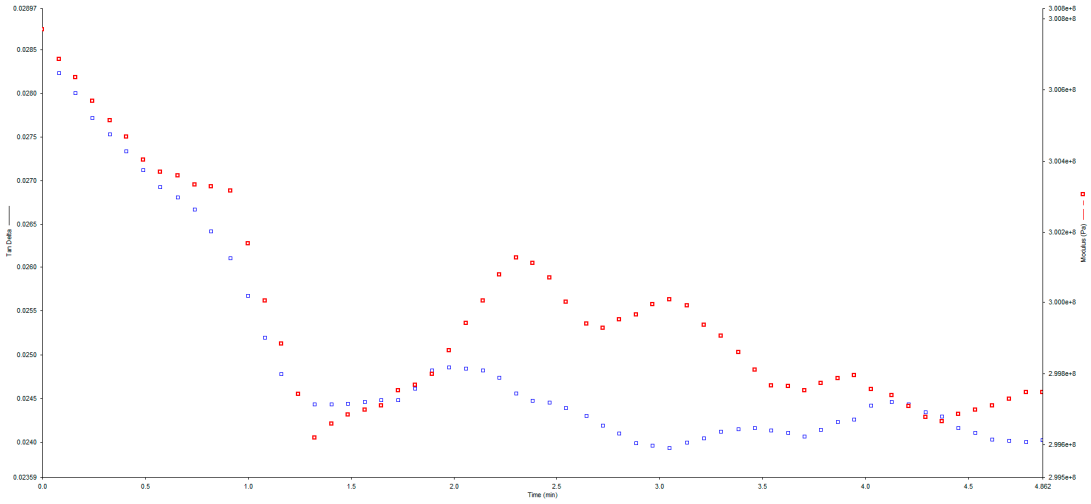


Figure 23. DMA results of samples tested at 300 °C.

The heated treatment sample to 350 °C is worth mentioning due to its decreasing modulus value (~3.47 × 10^8 Pa) (Figure 24). The tan δ curve was observed to increase

over time, indicating a partial recovery in the viscoelastic nature of the material. Hence, the above observations indicate that 350 °C is close to the material's thermal degradation temperature. At this temperature, mechanical properties are subject to loss as a result of chain breakage; oxidation or structural deterioration can also occur. Moreover, the increase in tan δ indicates an increase in internal friction and the conversion of energy within the material into heat. This means that unresolved internal structure deterioration somehow enhanced the viscoelastic property.

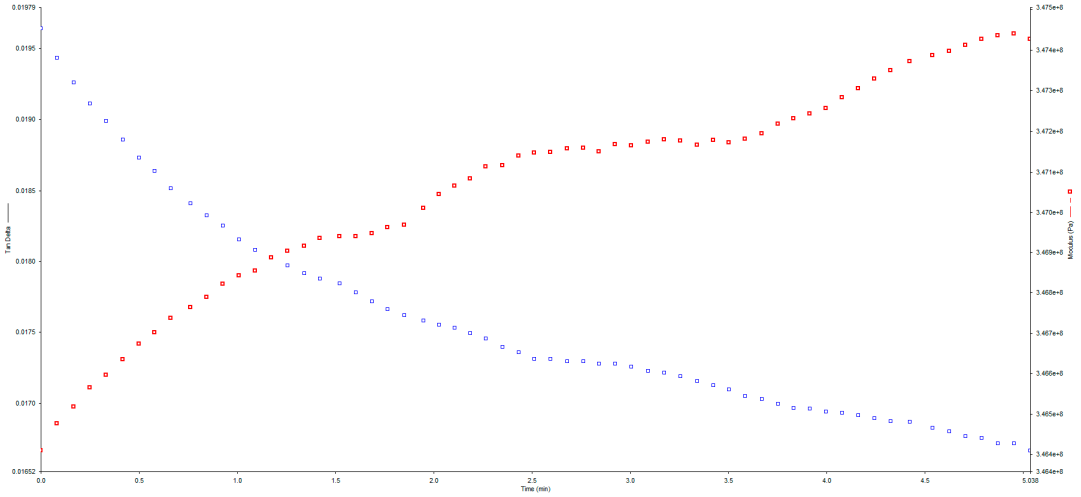


Figure 24. DMA results of samples tested at 350 °C.

3.2.4. Fourier Transform Infrared Spectroscopy (FT-IR) Results

Fourier Transform Infrared Spectroscopy (FT-IR) analysis was performed to determine the functional groups in the organic matrix structure of the composite samples (Figure 25). In this study, analysis was performed only on the reference sample (24 °C). The C–O–C and C–H bands in the spectrum belong to the core structural framework of the epoxy resin. In addition, the carbonyl peak at around 1730 cm^{-1} serves as an indicator of the putative cross-linking structure established after polymerization. Another possible interpretation of the broad –OH band in the 3300–3500 cm^{-1} region is the presence of resin-absorbed water or post-curing reaction residues. The visibility of the silica-based peaks (800–900 cm^{-1}) indicates that the glass fiber surface contributes to the FT-IR signal. This demonstrates that the matrix–fiber interface interaction can be analyzed.

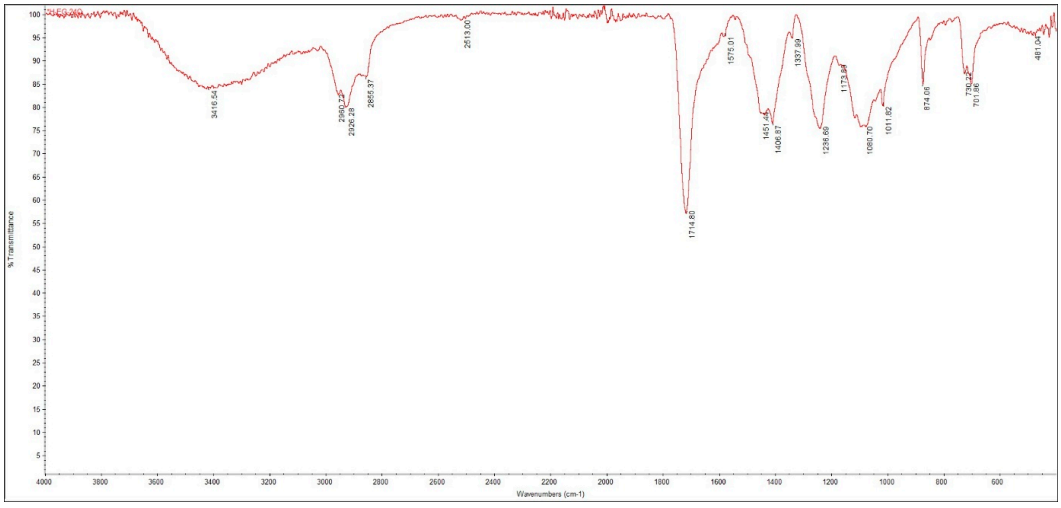


Figure 25. FT-IR results of samples tested at room temperature (24 °C).

3.3. Mechanical Tests

3.3.1. EG Loading Condition

All specimens exhibited fractures at the web–flange junction zones, regardless of temperature. This indicates that sudden shear and local buckling effects are decisive in the regions where load transfer is most concentrated.

The specimen tested at room temperature (24 °C) reached a maximum ultimate load of approximately 35 kN and exhibited a sudden post-elastic load drop on the load–displacement curve after a distinct elastic phase (Figures 26 and 27). Limited web buckling was observed at the start of loading, and microcracks and failures occurred at the upper web–flange junction starting at approximately 18 kN. As the load increased, these cracks deepened, causing crushing along the joint line, web fracture, and local separations.

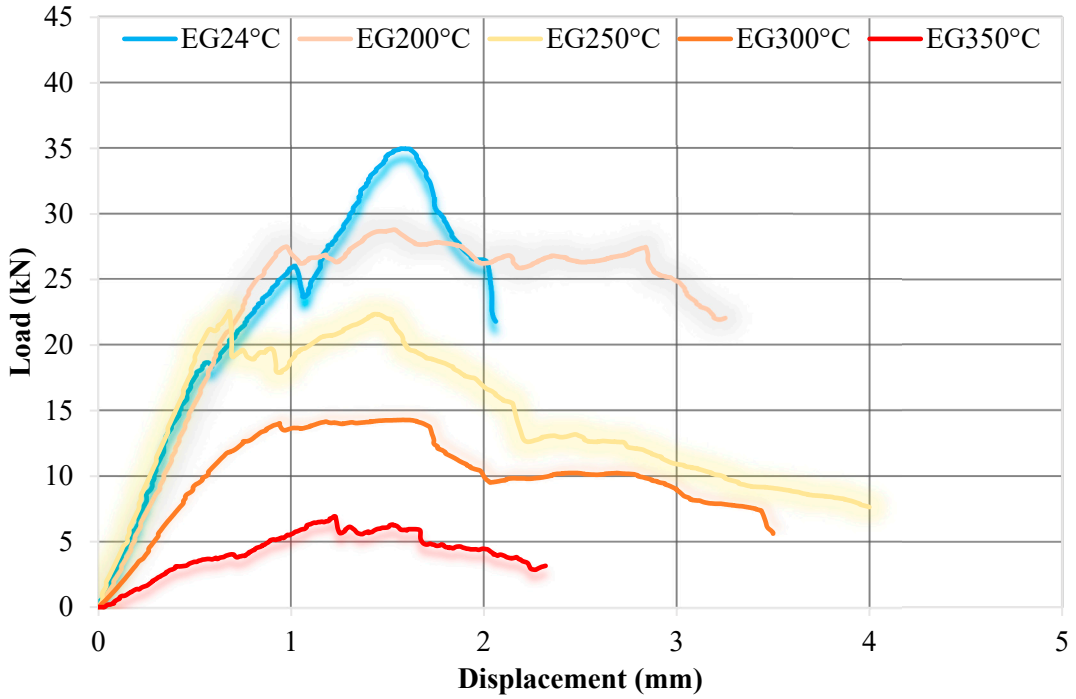


Figure 26. Load–displacement curve of specimens under EG with various temperatures.

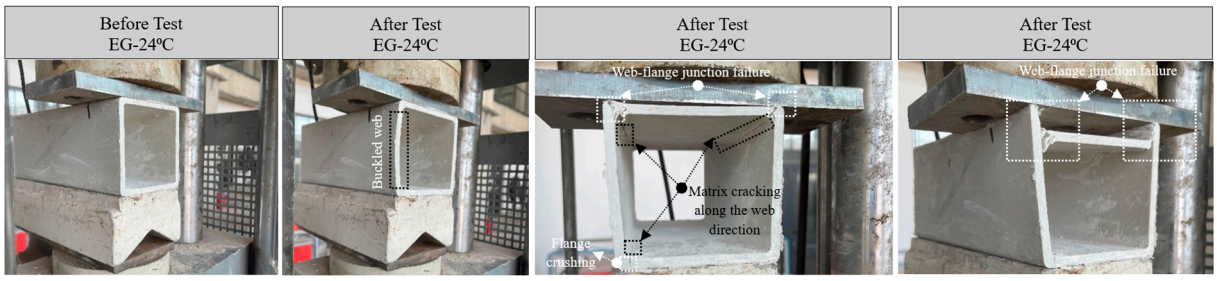


Figure 27. Failures of specimen EG24 °C.

The specimen heated to 200 °C reached an ultimate load of approximately 29 kN. At this temperature, the material still retained its partially elastic behavior, but 45° shear cracks developed in the web–flange junction, leading to localized failures (Figure 28).

The progressive damage evolution with increasing load is shown in Figure 28. At the start of the test, limited buckling occurred in the web, and matrix cracking in this region progressed in the load direction, reaching the web–flange junction zone. As the load increased, these cracks merged to form a crosswise crack line along the web direction,

followed by flange crushing and junction separation in the flange zone. In the final state, delamination and local crushing were observed at the junction line.

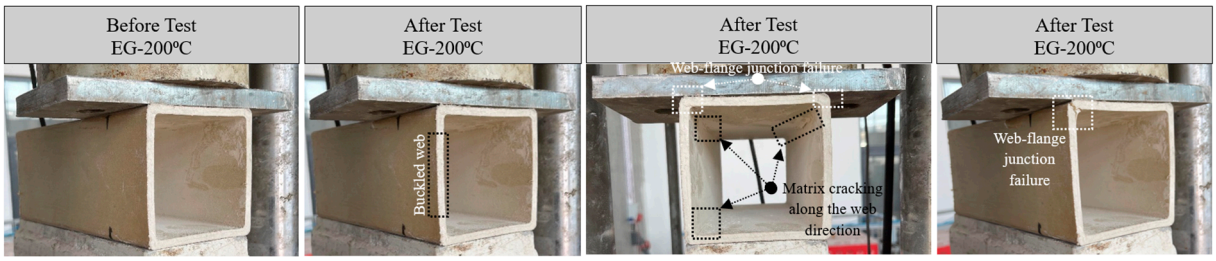


Figure 28. Failure of specimen EG200 °C.

Figure 28 shows that in the EG-200 °C specimen, the increase in temperature reduced the matrix stiffness, thereby weakening the adhesion at the fiber–matrix interface and increasing sensitivity to the shear effect. Consequently, this situation led to a fracture occurring at an earlier load.

The load-carrying capacity of the specimen exposed to 250 °C reached 22.55 kN. At this temperature, the material behavior became significantly brittle, and the elastic region of the load–displacement curve shortened.

With the increase in load, shear-induced damage development became dominant; cracking occurred at the web–flange junction and spread parallel to the loading direction to the middle of the web (Figure 29).

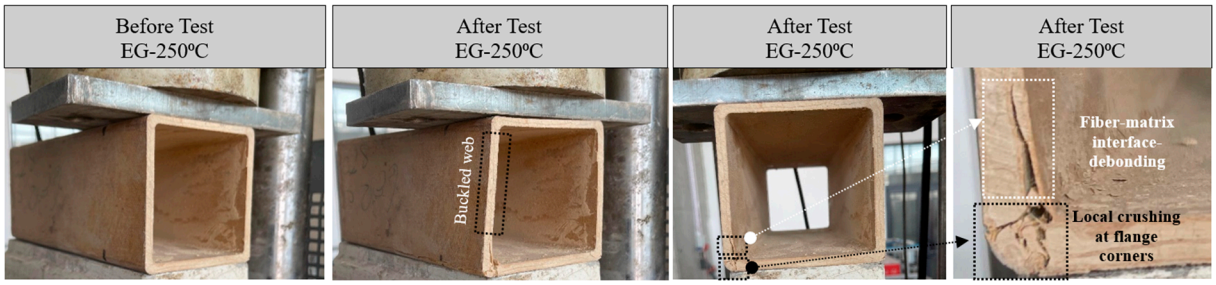


Figure 29. Failure of specimen EG250 °C.

As shown in Figure 29, damage progression initially began with web buckling and matrix cracking, followed by debonding at the fiber–matrix interface and the emergence of shear-oriented cracks at medium loads. As the ultimate load was approached, local crushing at flange corners and flange separation were observed; matrix debonding on the inner surface and resin discoloration/oxidation were noticeable.

Consequently, at 250 °C, the fracture mechanism was primarily characterized by sudden shear failure, with loss of fiber–matrix adhesion accelerating the reduction in load-carrying capacity.

Figure 30 shows the pre- and post- EG loading conditions of the pultruded GFRP hollow section specimen heated at 300 °C. The EG-300 °C specimen, exposed to 300 °C, exhibited a dramatic capacity loss of approximately 59% compared to the reference specimen at room temperature (34.99 kN), with a final experimental load of 14.29 kN. This capacity loss is directly related to the composite damage mechanisms shown in Figure 30. After loading, a distinct local buckling formed in the web region, and this buckling was the dominant damage mechanism in the reduction of the section's load-carrying capacity. Furthermore, the separation observed at the web–flange junction developed as a result of the decrease in resin hardness and the weakening of the fibre–matrix bond due to the

effect of temperature. The local crushing observed at the flange corners indicates that load transfer was concentrated in these areas and that the high temperature increased the resin fluidity, leading to stress accumulation. Furthermore, debonding at the fibre–matrix interface proves that the internal bond integrity of the composite material was significantly weakened under high temperatures. These damage patterns reveal that the effect of heat reduces the elastic modulus, particularly in resin-based composite systems, and limits local stability.

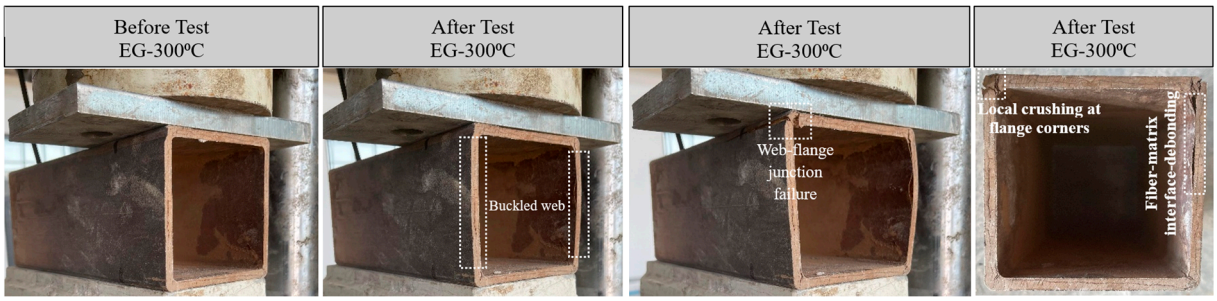


Figure 30. Failure of specimen EG300 °C.

In the pultruded GFRP section subjected to EG loading type and heated at 350 °C, the maximum load decreased from 34.99 kN to 6.92 kN compared to that at 24 °C. This corresponds to a decrease of approximately 80.2% in load capacity, showing that strength was reduced to one-fifth under the effect of heat. This significant decrease corresponds perfectly with the buckling of the web, the separation of the flange–web junction, the breaking of fibers, and the debonding of fibers from the matrix observed in Figure 31. This result shows that 350 °C is the critical thermal limit for pultruded GFRP systems and that above this temperature, degradation of the resin phase leads to a significant loss of composite interaction.

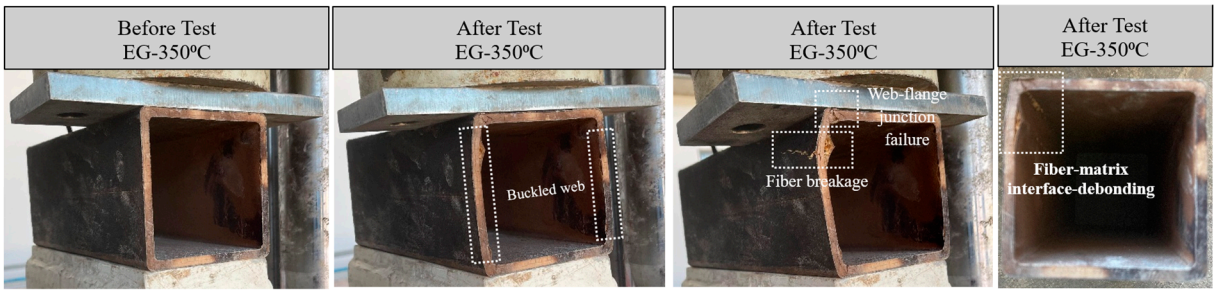


Figure 31. Failure of specimen EG350 °C.

3.3.2. IG Loading Condition

All specimens tested under IG loading conditions exhibited an initial failure mode in the web–flange junction region. However, upon analyzing the load–displacement curve (Figure 32) and failure modes (Figure 33), it is evident that the temperature exposure significantly affects both the ultimate load-carrying capacity and the failure modes. The ultimate capacity of the reference specimen (IG-24 °C), which was 40.37 kN, decreased to 9.76 kN at 350 °C (IG-350 °C), experiencing a critical capacity loss of 75.8% (Table 2).

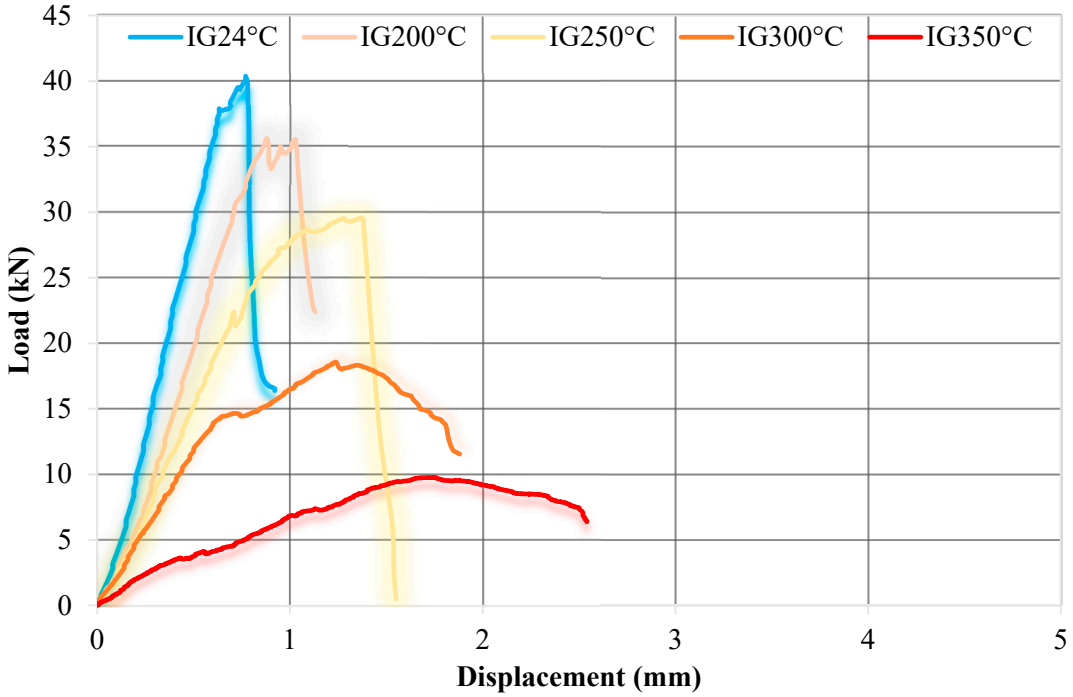
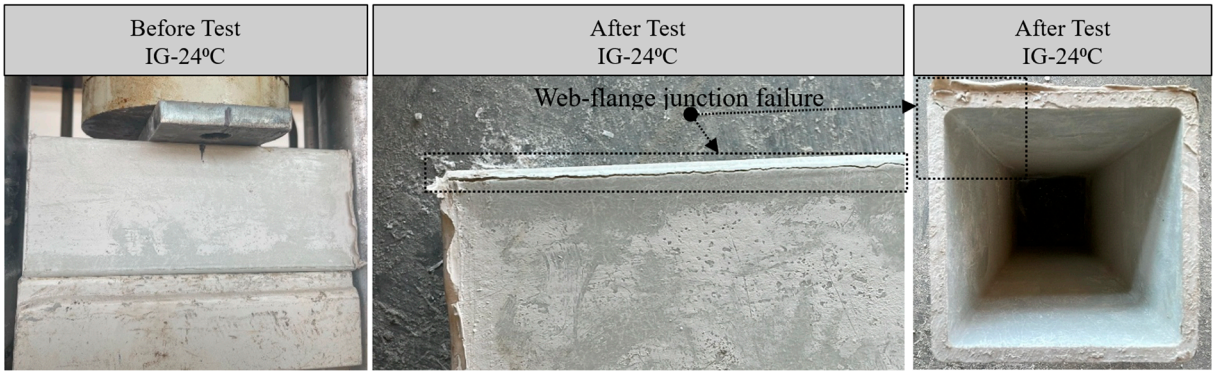
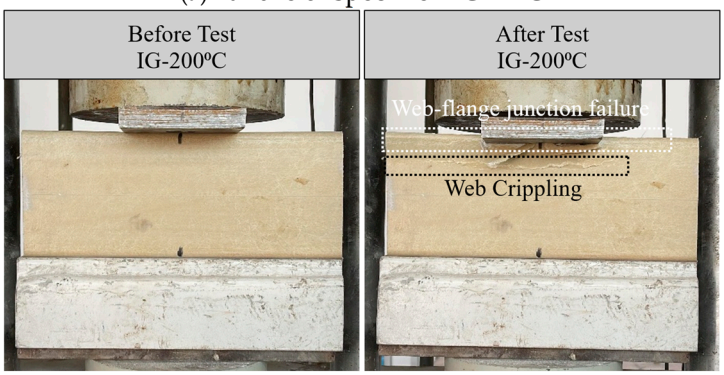


Figure 32. Load–displacement curve of specimens under IG with various temperatures.

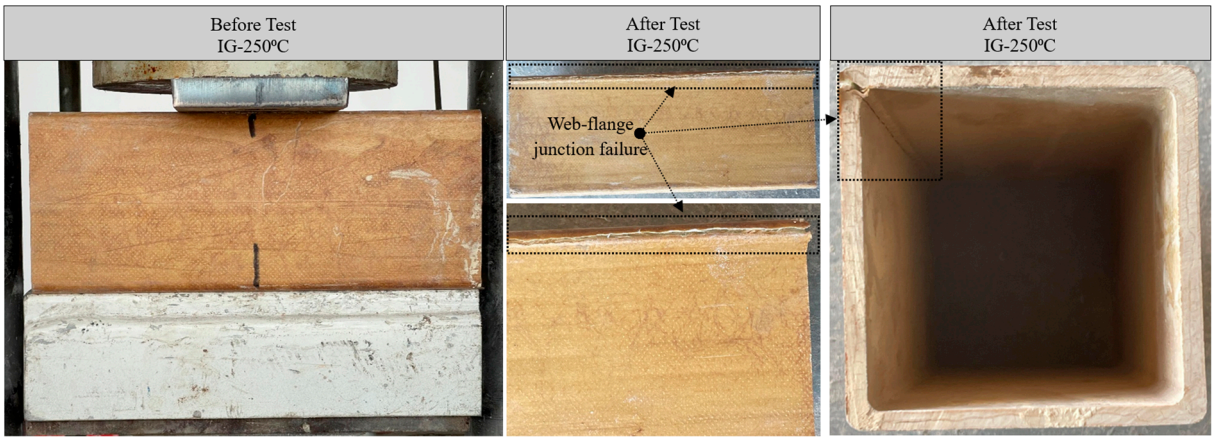


(**a**) Failure of specimen IG24 °C

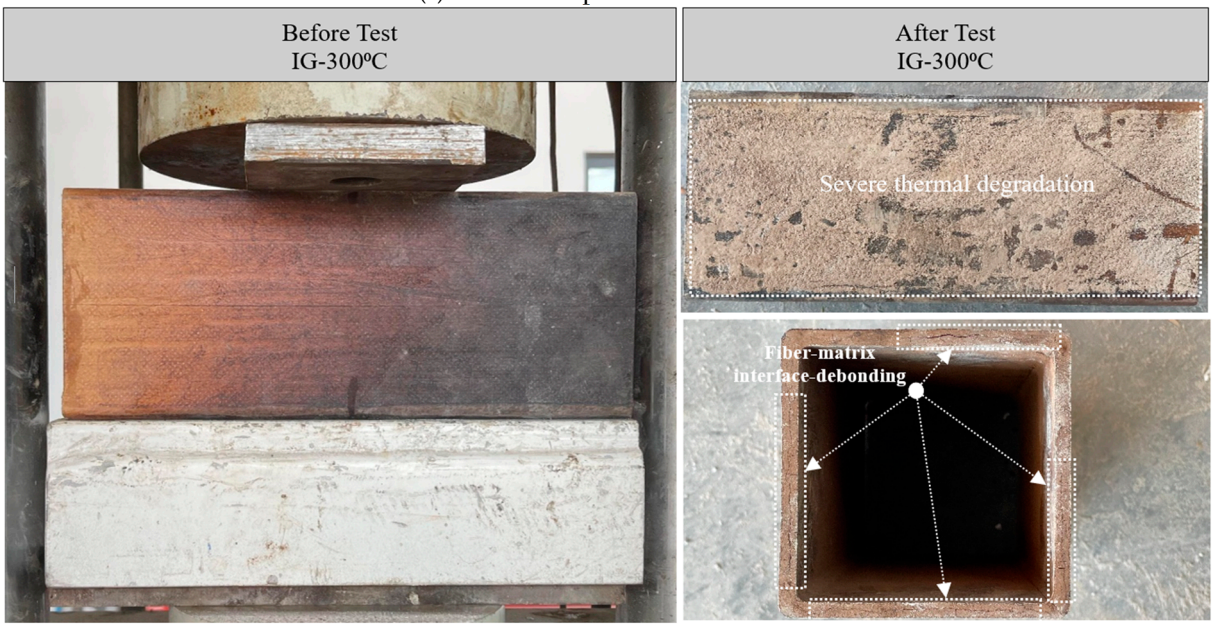


(**b**) Failure of specimen IG24 °C

Figure 33. *Cont.*



(**c**) Failure of specimen IG200 °C



(**d**) Failure of specimen IG200 °C



(**e**) Failure of specimen IG250 °C

Figure 33. Failure of specimen IG24, 200, 250, 300, 350 °C.

Table 2. Experimental and predicted results.

	Experimental Results (kN)					Predicted Results (kN)					Experimental/Predicted Results				
Test	**24 °C**	**200 °C**	**250 °C**	**300 °C**	**350 °C**	**24 °C**	**200 °C**	**250 °C**	**300 °C**	**350 °C**	**24 °C**	**200 °C**	**250 °C**	**300 °C**	**350 °C**
EG	34.99	28.80	22.55	14.29	6.92	35.8	28.5	22.4	14.5	4.8	0.98	1.01	1.01	0.99	1.45
ETF	33.30	25.95	21.03	13.14	6.73	33.5	26.7	21.0	13.5	4.5	0.99	0.97	1.00	0.97	1.51
IG	40.37	35.63	29.58	18.56	9.76	41.7	33.2	26.1	16.8	5.5	0.97	1.07	1.14	1.10	1.76
ITF	38.32	33.37	27.26	15.88	8.30	38.0	30.3	23.8	15.4	5.1	1.01	1.10	1.15	1.03	1.64

The reference specimen at room temperature (IG-24 °C) exhibited linear-elastic behavior with high stiffness up to approximately 38 kN, followed by a sudden load drop due to an abrupt brittle fracture at the web–flange junction beyond this load level (Figure 32). The damage was observed in the form of shear cracks concentrated in the region below the loading plate (Figure 33a).

In the specimen heated to 200 °C (IG-200 °C), the capacity decreased to 35.63 kN, and the behavior remained brittle. However, at this temperature, in addition to joint damage, significant web crippling and partial web–flange separation were observed (Figure 33b). This situation indicates that the fiber–matrix interface bond weakened as the matrix began to soften at 200 °C.

At 250 °C (IG-250 °C), a distinct change in behavior was observed. While the capacity dropped to 29.58 kN, the stiffness of the load–displacement curve (Figure 32) decreased and began to exhibit a more ductile (pseudo-ductile) behavior towards the peak load. This indicates that the matrix had softened significantly and that the damage had transformed into a progressive cracking mechanism (as seen in Figure 33c) that propagates along the joint region until a sudden fracture occurs.

The most noticeable change in behavior occurred in specimens exposed to 300 °C and 350 °C. The ultimate capacities decreased to 18.56 kN (54.0% loss) and 9.76 kN (75.8% loss), respectively. At these temperatures, the composite structure of the material underwent severe thermal degradation. The sharp drop in the slope (stiffness) of the curves in Figure 32 proves that the resin phase largely lost its load-transferring capacity. As a result, the damage mechanism shifted from brittle fracture to a pseudo-ductile failure mode characterized by excessive settlement and crushing due to complete degradation of the matrix (Figure 33d,e). The damage and load–displacement curve observed here should be evaluated as pseudo-ductility.

Consequently, under IG loading conditions, the temperature increase not only reduced the load-carrying capacity of the P-GFRP profiles but also transformed the damage mode from a stiff and brittle composite fracture to a pseudo-ductile behavior caused by thermal degradation.

3.3.3. ETF Loading Condition

Under the ETF loading condition, the specimens exhibited two main damage modes that differed significantly depending on temperature. At low temperatures, web buckling was predominant, while at high temperatures, crushing due to thermal degradation was observed. The ultimate load capacity decreased from 33.30 kN at 24 °C to 6.73 kN at 350 °C, representing a very significant loss of 79.8% (Table 3).

The specimen at room temperature (ETF-24 °C) exhibited linear behavior up to approximately 22 kN, after which distinct local buckling began in the web under transversal load (Figure 34). As the load continued to increase, this buckling led to expansion of the web and, consequently, to cracks both at the web–flange junctions (especially internally) and at the mid-height of the web. Final failure occurred at a load level of 33.30 kN with web rupture (Figure 35a).

Table 3. Equations for predicting ultimate load under ETF and ITF, EG, and IG loading conditions for PGFRP.

For EG loading conditions	$0.9\zeta\left(3-\frac{H-2t_f}{100t_w}\right)\left(1+0.02\frac{b}{t_w}\right)t_w^2 f_y$
For IG loading conditions	$0.9\zeta\left(3-\frac{H-2t_f}{50t_w}\right)\left(1+0.02\frac{b}{t_w}\right)t_w^2 f_y$
For ETF loading conditions	$0.9\zeta\left(4-\frac{H-2t_f}{30t_w}\right)\left(1+0.002\frac{b}{t_w}\right)t_w^2 f_y$
For ITF loading conditions	$0.9\zeta\left(4-\frac{H-2t_f}{20t_w}\right)\left(1+0.002\frac{b}{t_w}\right)t_w^2 f_y$

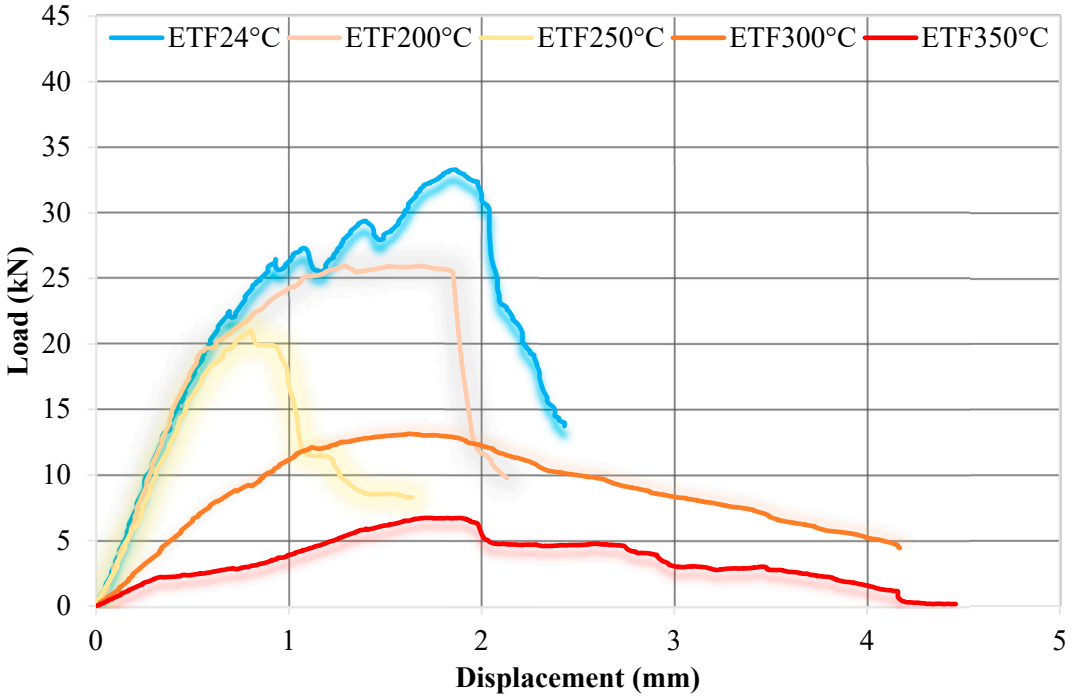
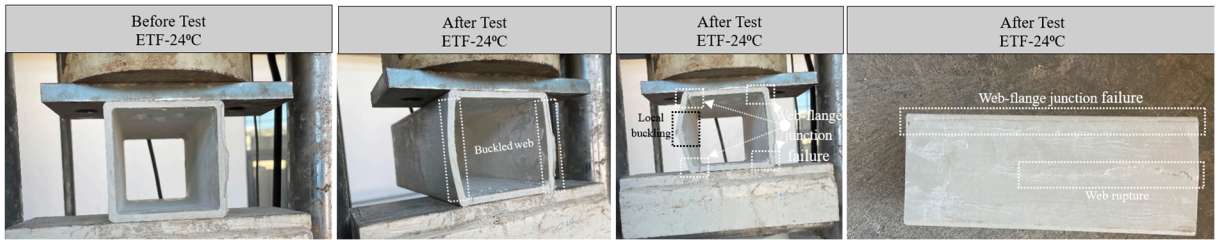


Figure 34. Load–displacement curve of specimens under ETF with various temperatures.

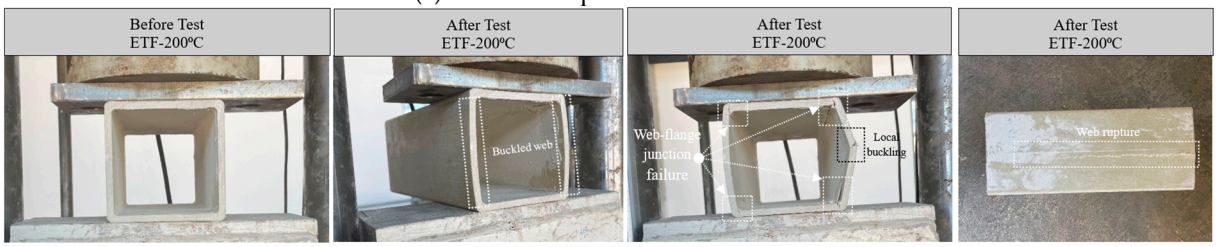
The specimen heated to 200 °C (ETF-200 °C) exhibited a similar buckling-induced damage mode and reached a final load of 25.95 kN. The damage manifested as fractures at mid-height of the web and deepening cracks at the junctions (Figure 35b).

At 250 °C (ETF-250 °C), a capacity of 21.03 kN was achieved. At this temperature, with the material stiffness beginning to decrease, the damage mode transformed into a combination of buckling and sudden junction fracture (Figure 35c).

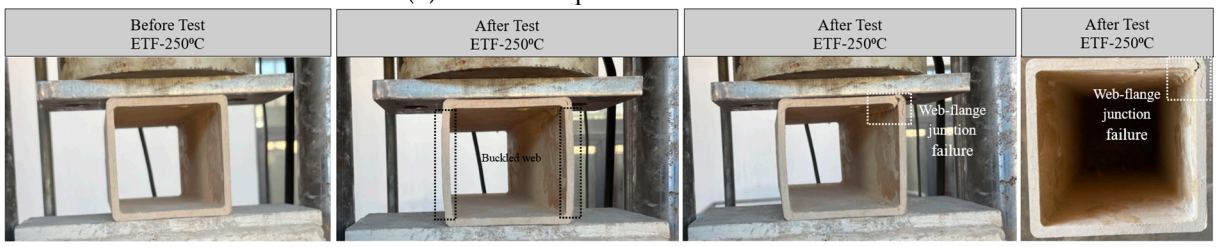
The behavior changed completely at 300 °C and above. The 300 °C (ETF-300 °C) specimen reached a capacity of 13.14 kN, while the load–displacement curve (Figure 34) took on a parabolic shape, indicating severe degradation of the matrix. The failure mode occurred at the corner points as web–flange failure due to local buckling and excessive settlement (Figure 35d). Fiber–matrix interface debonding damage was also observed. At 350 °C (ETF-350 °C), the capacity dropped to 6.73 kN, while the specimen exhibited almost no stiffness and showed excessive displacement. Figure 35e clearly shows that the laminate layers detached and the profile was completely crushed due to the complete decomposition of the resin, without any buckling.



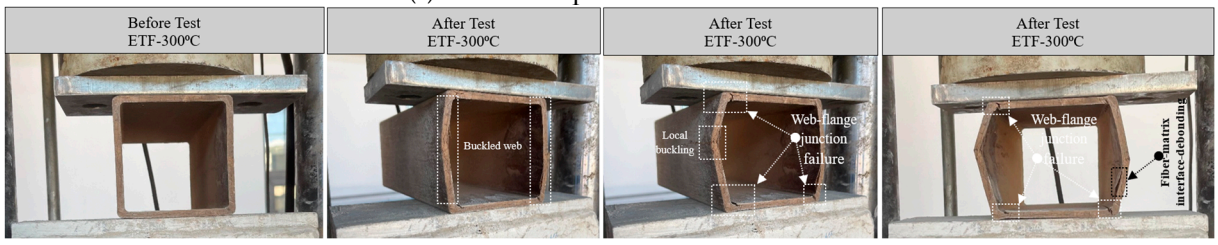
(**a**) Failure of specimen ETF 24 °C



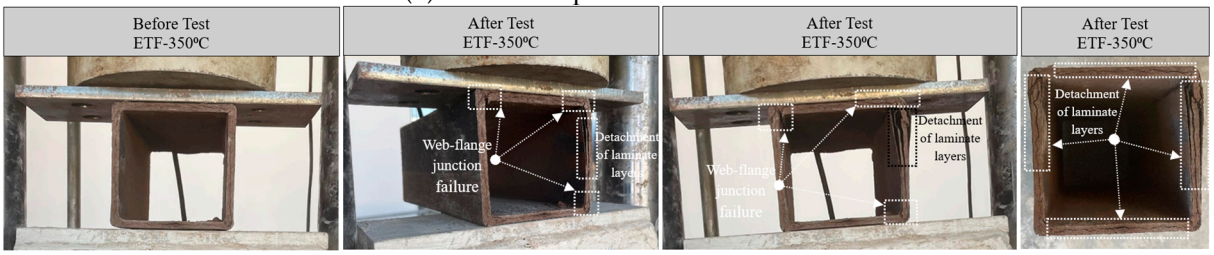
(**b**) Failure of specimen ETF 200 °C



(**c**) Failure of specimen ETF 250 °C



(**d**) Failure of specimen ETF 300 °C



(**e**) Failure of specimen ETF 350 °C

Figure 35. Failure of specimen ETF24, 200, 250, 300, 350 °C.

3.3.4. ITF Loading Condition

The ITF loading condition exhibits the most complex damage mechanism development depending on temperature. Damage modes showed a transition between brittle web–flange junction fracture at low temperatures and web rupture at medium temperatures; thermal degradation became dominant at high temperatures. The ultimate load capacity decreased from 38.32 kN at 24 °C to 8.30 kN at 350 °C, representing a significant capacity loss of 78.3% (Table 3).

The reference specimen at room temperature (ITF-24 °C) exhibited high stiffness behavior up to 38 kN and experienced sudden and brittle failure upon reaching the peak load (38.32 kN) (Figure 36). This behavior is confirmed by the sharp drop in load shown in Figure 36 (blue curve). The damage that occurred initially took the form of an abrupt

separation at the web–flange junction in the lower section (Figure 37a). Subsequently, as the load increased, crushing and fiber breakage were observed at the loading points.

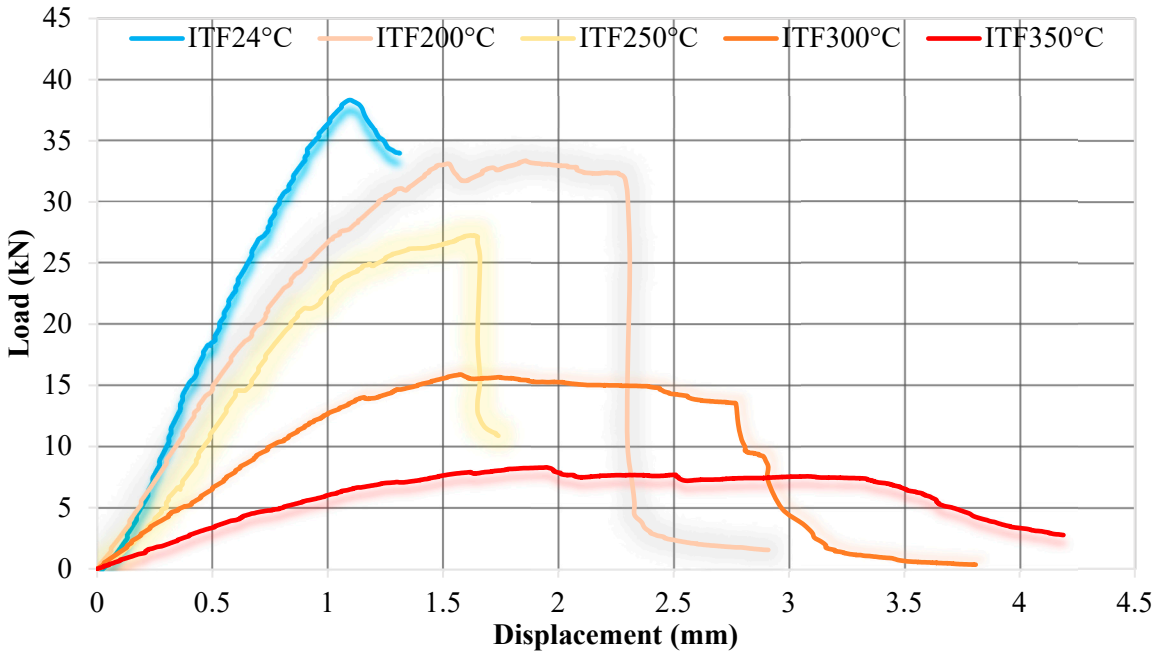


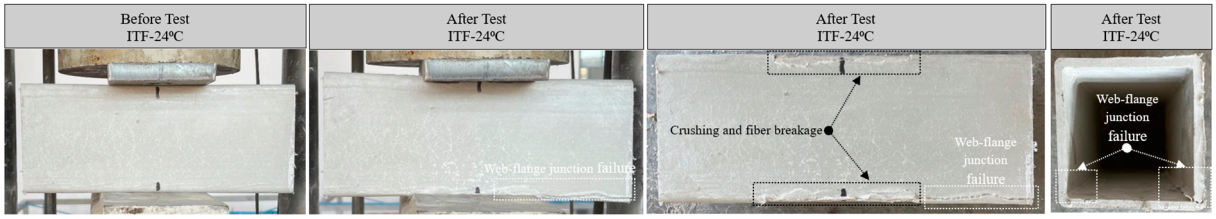
Figure 36. Load–displacement curve of specimens under ITF with various temperatures.

Heating to 200 °C (ITF-200 °C) significantly altered the damage mode. The ultimate capacity decreased to 33.37 kN. Unlike brittle joint failure, the dominant damage mode in this specimen was tearing/fracturing at the mid-height of the web (web fracture), as clearly seen in the photographs in Figure 37b. The post-peak plateau observed after the peak load in the graph in Figure 36 (pink curve) confirms this non-sudden, progressive web fracture.

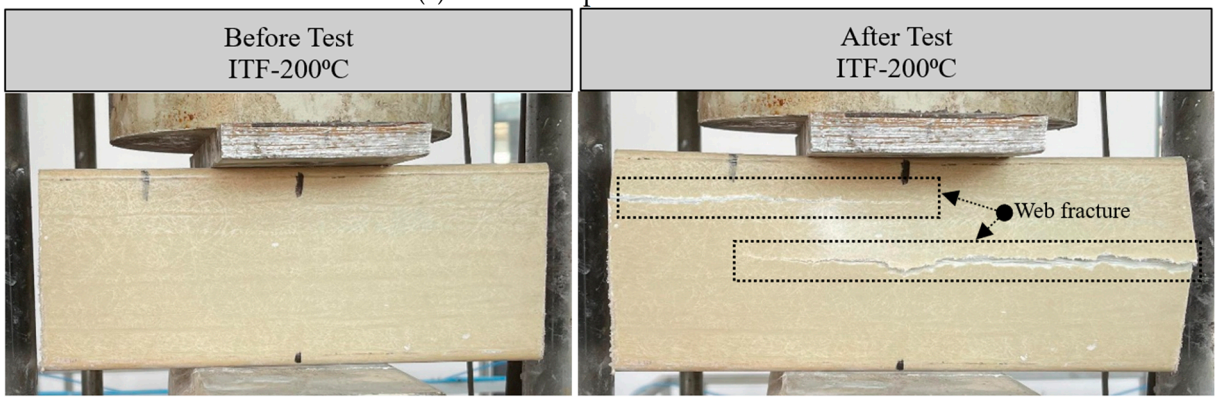
Interestingly, at 250 °C (ITF-250 °C), the damage mode reverted to brittle behavior. The capacity dropped to 27.26 kN, and as shown by the sharp load drop in Figure 36 (purple curve), the specimen experienced an abrupt loss of capacity at peak load. This is consistent with the crack images in Figure 37c. Upon examination of Figure 37c, it is observed that as the load increased, web fracture first occurred below the upper loading point, and this damage then propagated and expanded towards the right and left ends of the specimen. Web–flange junction failure was also observed.

The specimen exposed to 300 °C (ITF-300 °C) reached a final load capacity of 15.88 kN (Table 3). At this temperature, a significant loss in material stiffness is observed. The load–displacement curve in Figure 36 (light red) exhibited a long plateau after reaching the peak load, unlike the sudden brittle fracture at 250 °C. This pseudo-ductile behavior indicates that thermal degradation changed the damage mode. The resulting damage mechanism is no longer an abrupt junction fracture, but rather occurs as the load is damped by the web and as 'excessive web buckling and rupture' at different heights (Figure 37d).

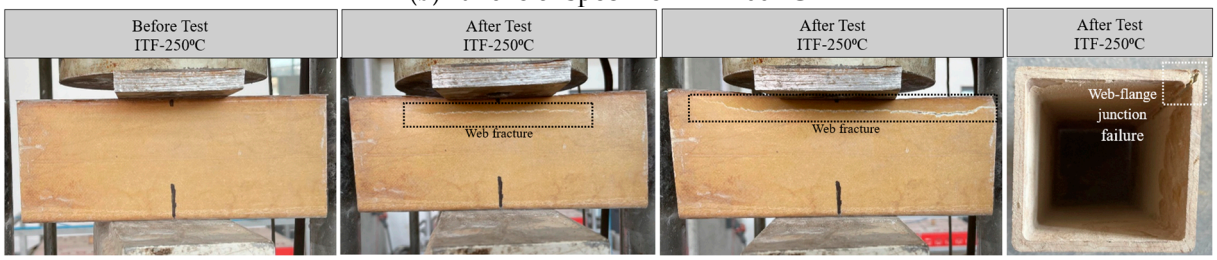
At 350 °C (ITF-350 °C), the structural integrity of the composite material was largely lost due to the almost complete degradation of the resin matrix. The ultimate capacity dropped to 8.30 kN, the lowest value among all conditions (Table 3). The curve in Figure 36 (dark red) exhibited excessive displacement behavior under an almost constant load. This proves that the stiffness was completely lost and that the damage mode transformed into a pseudo-ductile mode that could be described as progressive crushing. The cross-sectional photographs in Figure 37e clearly show that the profile can no longer carry the load, is completely crushed, and has delaminated.



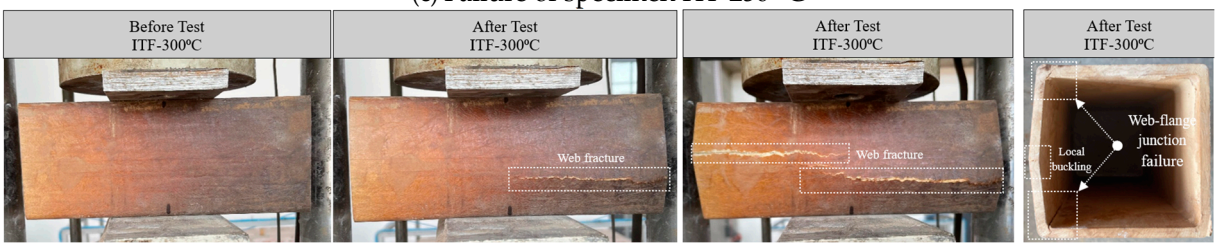
(**a**) Failure of specimen ITF 24 °C



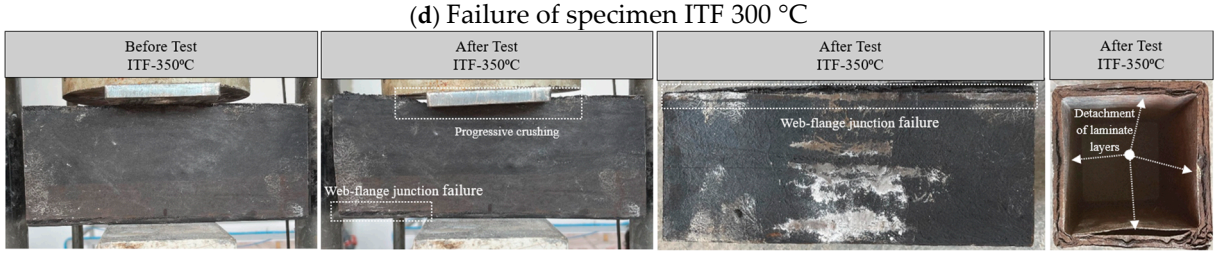
(**b**) Failure of specimen ITF 200 °C



(**c**) Failure of specimen ITF 250 °C



(**d**) Failure of specimen ITF 300 °C



(**e**) Failure of specimen ITF 350 °C

Figure 37. Failure of specimen ITF24, 200, 250, 300, 350 °C.

3.3.5. Comparison of Loading Conditions

Test results indicate that loading conditions (configuration) have a critical effect on web crippling behavior, comparable to temperature. Four different loading conditions (EG, IG, ETF, ITF) exhibited distinct differences in both ultimate capacity and failure mode.

At all temperatures (from 24 °C to 350 °C), a consistent relationship was observed between the ultimate load-carrying capacities (P) of the specimens. This relationship is P(IG) > P(ITF) > P(EG) > P(ETF) (Table 3). Two main factors influenced this ranking. First, Interior loads (IG and ITF) systematically yielded higher capacities than End loads

(EG and ETF). For example, at 24 °C, P_{IG} (40.37 kN) is approximately 15% higher than P_{EG} (34.99 kN). This can be explained by the fact that 'End' loads are applied at the end of the profile, where stress concentration is critical, while 'Internal' loads distribute the load over a wider web area. Secondly, under both 'Interior' and 'End' conditions, specimens loaded with 'Plate and Ground' (IG and EG) exhibited higher capacity than those loaded with 'Two Plates' (ITF and ETF) (e.g., P(IG) > P(ITF) > P(EG) > P(ETF)).

The loading configuration directly affected not only the capacity but also the stiffness and ductility of the material. As seen in Figure 38 (24 °C), IG and ITF interior loadings exhibited significantly higher stiffness (steeper slope) and more brittle behavior. These specimens failed abruptly at low displacement values (~0.7–1.2 mm), experiencing sudden capacity loss. In contrast, the EG and ETF specimens exhibited lower stiffness and a pronounced plastic/elastoplastic plateau after the peak load, demonstrating a much more ductile (pseudo-ductile) behavior. These specimens failed at relatively higher displacements (~1.6–1.8 mm). This finding is significant for practical applications. In other words, although 'End' loadings have lower capacity, they provide A warning by deforming more before yielding (pseudo-ductile behavior).

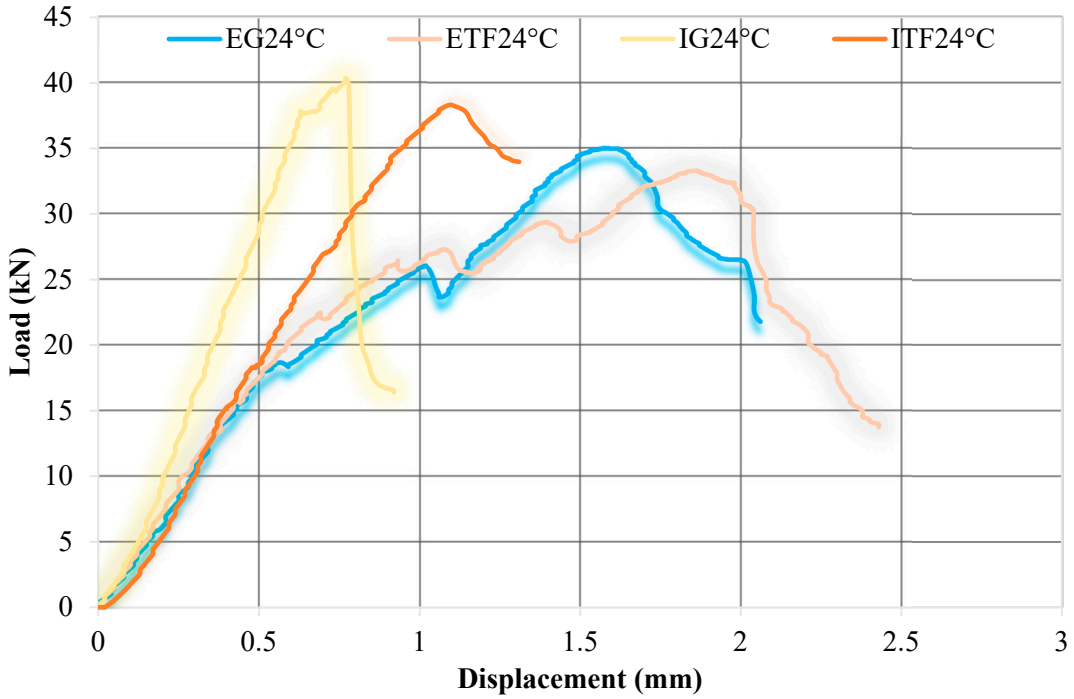


Figure 38. Comparison of specimens subjected to a temperature of 24 °C under different loading conditions.

When the temperature increased to 200 °C and 250 °C, these fundamental behavioral differences (inner-brittle, outer-ductile) were largely preserved (Figures 39 and 40). However, at extremely high temperatures such as 300 °C and 350 °C (Figures 41 and 42), the behaviors converge. At these temperatures, severe thermal degradation of the resin matrix eliminates composite interaction. Consequently, regardless of the loading condition, all specimens exhibited a low-stiffness, pseudo-ductile/plastic-like failure behavior characterized by 'excessive settlement'.

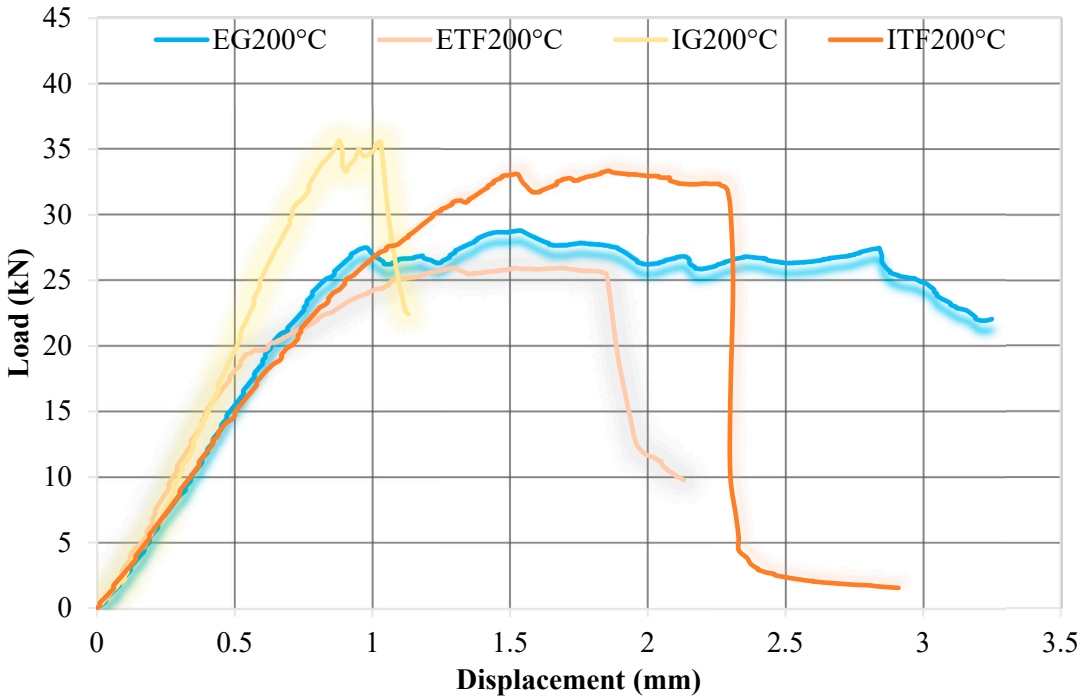


Figure 39. Comparison of specimens subjected to a temperature of 200 °C under different loading conditions.

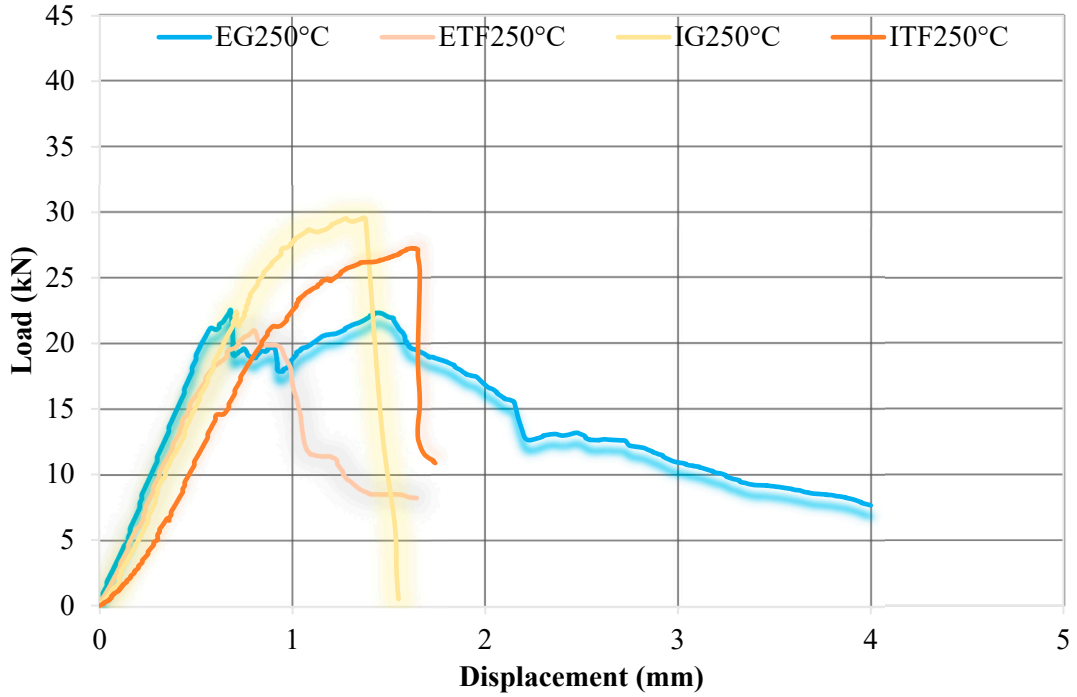


Figure 40. Comparison of specimens subjected to a temperature of 250 °C under different loading conditions.

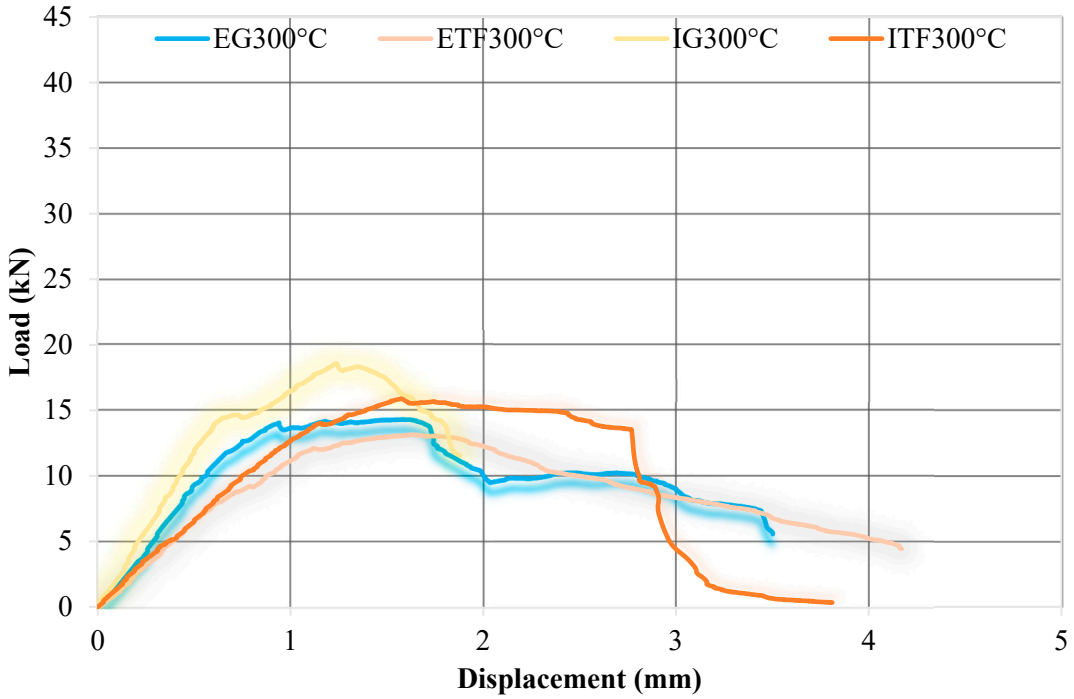


Figure 41. Comparison of specimens subjected to a temperature of 300 °C under different loading conditions.

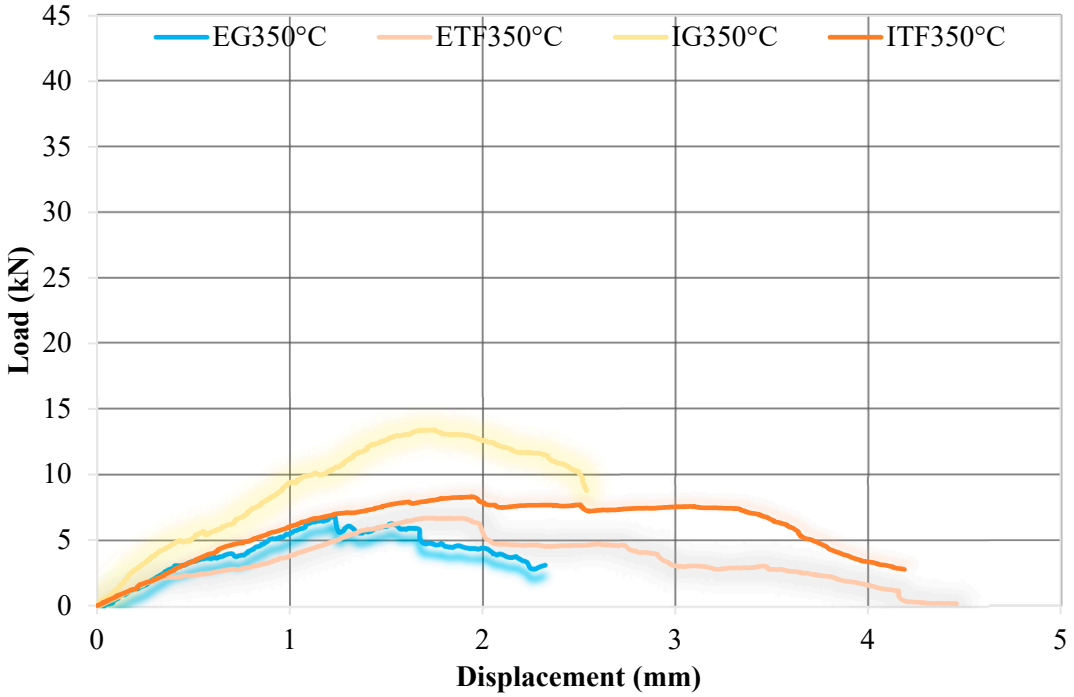


Figure 42. Comparison of specimens subjected to a temperature of 350 °C under different loading conditions.

3.3.6. Comparison of Thermal Effect

As indicated in many other studies we reviewed in the literature, as well as in our work, the ultimate loads of the specimens decreased as they were subjected to increasingly higher temperatures (Figures 43 and 44). The experimental results clearly indicate that the ultimate web crippling load of pultruded GFRP hollow sections exhibits a nonlinear decreasing trend with temperature under all loading configurations. This degradation can

be attributed to the combined effects of matrix decomposition, fiber–matrix debonding, and softening of the resin phase beyond the glass transition temperature (Tg ≈ 140 °C), as confirmed by DMA and TGA analyses. To quantitatively predict this thermal reduction, empirical equations were derived for the web crippling behavior of pultruded hollow box sections, regardless of loading configuration (EG, IG, ETF, and ITF). The following Equation (1) was developed in order to predict the effect of temperature:

$$\zeta = -0.00001 \times (T - 24)^2 + 0.0006 \times (T - 24) + 1 \quad (1)$$

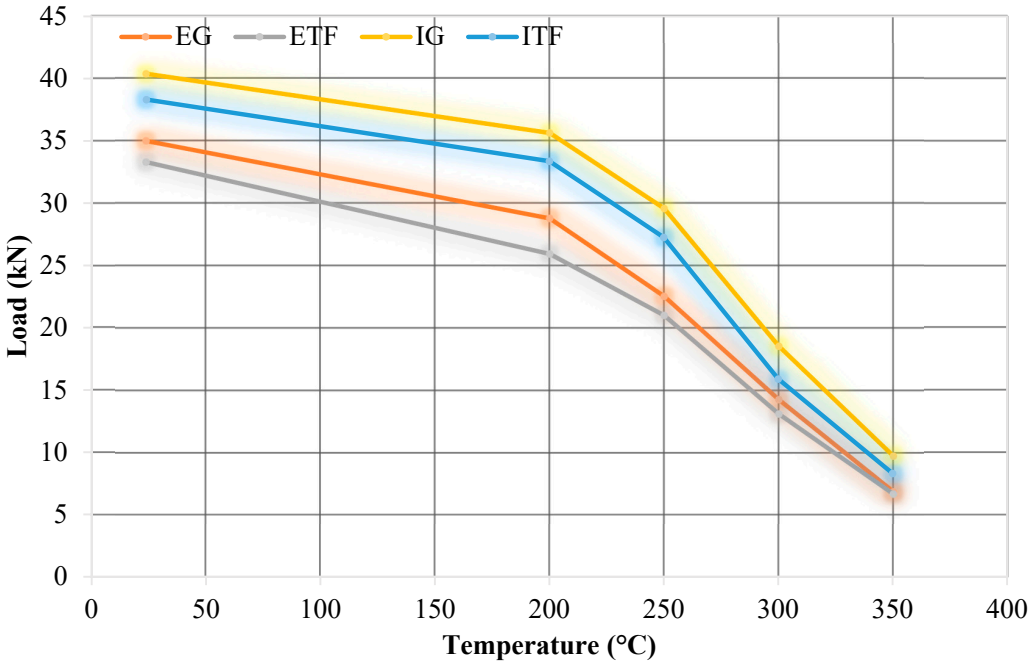


Figure 43. Load-temperature graphs with comparison of thermal effects.

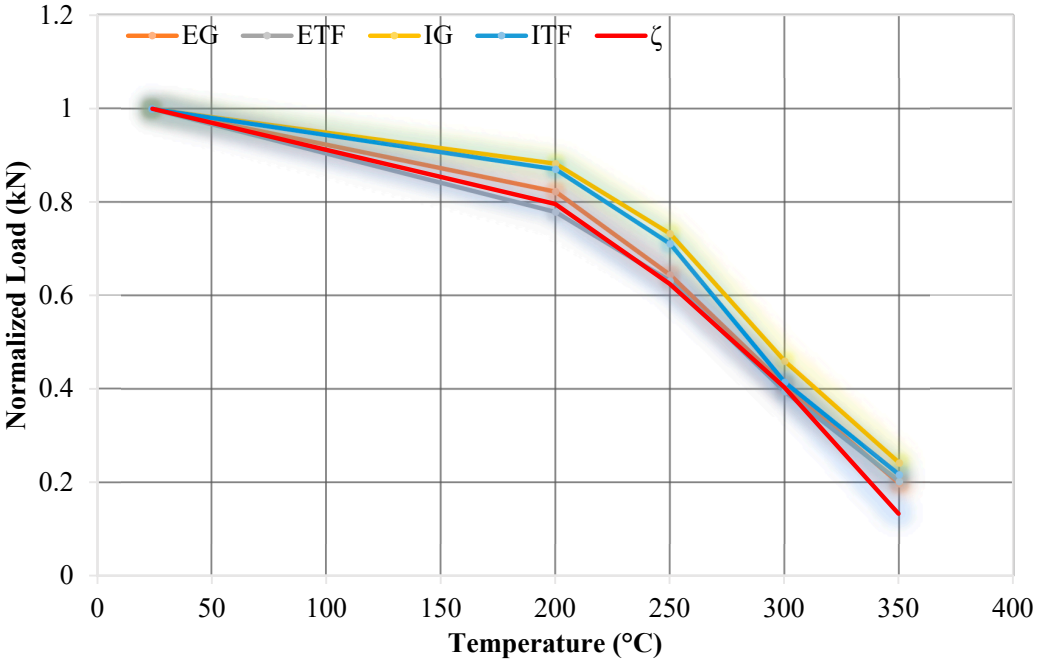


Figure 44. Normalized Load-temperature graphs with comparison of thermal effects.

The equation predicts a very limited increase up to approximately 54 °C, which is related to post-curing and the rearrangement of polymer chains occurring in the region below the glass transition temperature of the epoxy matrix. Above 54 °C, however, a continuous decrease in capacity is observed due to matrix softening, weakening of the fiber–matrix interface, and thermal degradation effects as the temperature increases. The model's predictions show good agreement with experimental results. For example, under EG loading conditions, the experimental load ratios at 200 °C, 250 °C, 300 °C, and 350 °C were measured as 0.82, 0.64, 0.41, and 0.20, respectively; the model predicted these values as 0.80, 0.63, 0.40, and 0.13, respectively. The average absolute error in the range of 24–300 °C is below approximately 3%, indicating that the model is quite reliable in this temperature range. At 350 °C, the increase in the difference is due to the advanced degradation of the epoxy resin at this temperature, and to the fact that delamination and carbonization cannot be fully represented by a single second-order function. Under internal loading conditions (IG and ITF), the capacity reduction remained lower; this indicates that internal loading distributes stresses more evenly and delays local buckling in thermally weakened sections. Furthermore, the trends predicted by the model are in full agreement with the softening and oxidation behavior of the epoxy matrix observed in DMA and TGA analyses.

4. Prediction of Load Capacity

In this study, equations predicting the load-carrying capacity were developed by considering not only the temperature effect but also the loading condition, geometric parameters, and experimental observations. These equations, given in Table 3, were formulated based on the current web crippling capacity formulations proposed by researchers such as [35]. However, these models were modified to include both the temperature effect (ζ) and the behavior differences associated with the loading configuration, in order to be consistent with the experimental results of the present study.

The comparisons in Table 2 show that the estimated capacity values obtained with these new equations are in high agreement with the experimental results. Specifically, within the 24–300 °C range, the experimental/predicted ratios ranged from 0.97 to 1.15, demonstrating the reliability of the model. At temperatures above 350 °C, however, significant drops in experimental values were observed due to the advanced degradation of the epoxy matrix; in contrast, the prediction equations reflected this situation conservatively. In conclusion, the modified equations presented in Table 3 encompass not only the temperature effect but also the combined effects of loading configuration and geometric variables; thus, they enable accurate prediction of the web crippling capacity of pultruded GFRP profiles over a wide range of parameters.

5. Conclusions

In this experimental study, the effects of elevated temperatures (from room temperature (24 °C) to 350 °C) and four different loading configurations (EG, IG, ETF, ITF) on web crippling behavior were investigated. The main findings and results obtained from comprehensive tests on 20 specimens are presented below:

1. Rising temperature caused significant decreases in the ultimate load-carrying capacity of the specimens due to thermal degradation of the composite matrix. The greatest loss was recorded at approximately 79.8% at 350 °C under the ETF loading condition.
2. 350 °C was determined to be the critical thermal limit for pultruded GFRP sections. At this temperature, the material's structural integrity was largely lost due to the almost complete degradation of the resin phase. It was determined that heating the specimens above this temperature would not be beneficial.

3. At low and medium temperatures (24–300 °C), the dominant failure mode was generally sudden, brittle fracture or web buckling; at high temperatures (300–350 °C), this mechanism transformed into pseudo-ductile behavior characterized by low stiffness, excessive collapse, and crushing due to the loss of matrix hardness.
4. Regardless of the temperature level, initial damage consistently occurred at the web–flange junctions. This confirms that these zones are critical points with the highest stress concentration.
5. A consistent order was observed among the ultimate capacities of the specimens: P(IG) > P(ITF) > P(EG) > P(ETF). This situation showed that Interior (IG, ITF) loadings, where the load is distributed over a wider web area, always provide higher capacity than End (EG, ETF) loadings.
6. At room temperature, Interior loadings (IG, ITF) exhibited higher stiffness and brittle behavior, while End loadings (EG, ETF) exhibited lower stiffness but more ductile (pseudo-ductile) behavior. This pseudo-ductile behavior is driven by geometric instabilities, such as localized web buckling permitted by the free edges in end configurations, rather than material yielding. This pseudo-ductile behavior indicates that sufficient ductility cannot be claimed regardless of the loading type.
7. At extremely high temperatures such as 300 °C and 350 °C, with thermal degradation becoming dominant, the behavioral differences between different loading conditions disappeared. All specimens exhibited low stiffness and a pseudo-ductile/plastic-like, progressive crushing collapse due to severe degradation of the matrix.
8. Significant changes in composite behavior (e.g., increased sensitivity to shear and decreased matrix stiffness) began at 200 °C, and a distinct transition from brittle fracture to progressive damage was observed, particularly at 250 °C.
9. High temperatures caused resin softening, weakening the adhesion at the fiber–matrix interface. This increased susceptibility to shear effects and led to separations (delamination/debonding), particularly at web–flange junctions.
10. A temperature-dependent reduction factor (ζ) was formulated to express the deterioration of web crippling resistance with temperature. The proposed empirical equations, incorporating ζ and loading configuration parameters, predicted the ultimate capacity with high reliability, yielding experimental-to-predicted ratios between 0.97 and 1.15 for the 24–300 °C range. At 350 °C, discrepancies increased due to severe matrix carbonization and delamination, which cannot be fully represented by a single polynomial function.

6. Future Studies

1. Future design provisions for pultruded GFRP structures should incorporate temperature-dependent capacity reduction factors and account for loading configuration effects to achieve safer and more reliable structural performance under fire conditions.
2. It should be emphasized that the present tests represent the residual web crippling capacity of pultruded GFRP hollow sections after elevated-temperature exposure and cooling. Testing under hot-state conditions would likely result in lower capacities due to matrix softening, reduced fiber–matrix bonding, and increased viscoelastic deformation during loading. Therefore, future studies should include hot-state web crippling tests to better simulate real fire and sustained service-temperature conditions.
3. It should be noted that the proposed prediction model was developed based on the tested 100 mm × 100 mm pultruded GFRP hollow section with a specific wall thickness, bearing arrangement, and fiber architecture. Future studies should expand the experimental database by considering different cross-sectional dimensions, bear-

ing lengths, fiber volume fractions, and laminate architectures to establish a more generalized design equation.

4. The higher load-carrying capacity observed under the IG loading condition can be attributed to the larger effective load transfer area and reduced local stress concentration compared with end-loading configurations. However, since strain field measurements, digital image correlation, or finite element stress analyses were not performed in this study, this explanation should be interpreted as mechanically plausible, based on the experimental load capacity and failure observations, rather than as direct strain field evidence. Future studies should include DIC measurements or validated finite element models to quantify the stress distribution and strain localization mechanisms under different loading configurations.
5. The proposed temperature-dependent reduction factors provide a practical representation of the ultimate load behavior under various loading conditions (ETF, ITF, EG, and IG); however, further validation using independent external experimental datasets is recommended to ensure generalizability

From a practical design perspective, 300 °C may be considered a critical warning level for the tested pultruded GFRP hollow section, as considerable matrix degradation and web crippling capacity loss were observed beyond this temperature. Exposure to 350 °C caused severe deterioration and should be avoided in structural applications without adequate fire protection. Therefore, engineers should apply temperature-dependent reduction factors, use conservative safety margins, and provide passive fire protection systems when pultruded GFRP profiles are used in fire-prone or high-temperature environments. These threshold values should be regarded as material- and geometry-specific rather than universal design limits.

From an engineering design perspective, the findings indicate that elevated temperatures can significantly reduce the web crippling resistance of pultruded GFRP hollow sections, particularly above 250–300 °C. Therefore, temperature-dependent reduction factors should be incorporated into design calculations when these members are intended for service in fire-prone or high-temperature environments. The results also demonstrate that loading configuration has a considerable influence on load-carrying capacity, suggesting that designers should carefully consider load introduction details and bearing arrangements during the design stage. For practical applications, the use of passive fire protection systems, thermal insulation coatings, or protective cladding is recommended to delay matrix degradation and preserve structural integrity during fire exposure. Furthermore, pultruded GFRP members used in critical infrastructure should be evaluated using performance-based fire design approaches to ensure adequate safety under elevated-temperature conditions.

Author Contributions: Conceptualization, E.M. and Y.O.Ö.; methodology, C.A., E.M. and Y.O.Ö.; validation, M.A.S., E.M. and Y.O.Ö.; formal analysis, M.A.S.; investigation, M.A.S.; resources, Y.O.Ö.; data curation, E.M. and Y.O.Ö.; writing—original draft preparation, M.A.S.; writing—review and editing, E.M., C.A. and Y.O.Ö.; visualization, Y.O.Ö.; supervision, Y.O.Ö.; project administration, Y.O.Ö. All authors have read and agreed to the published version of the manuscript.

Funding: This study has been supported by the Department of Scientific Research Projects at Necmettin Erbakan University with the project coded 24YL19007.

Data Availability Statement: The data will be provided upon request from the corresponding author.

Acknowledgments: During the preparation of this work, the authors used ChatGPT 5 in order to improve several important aspects of writing, such as readability, grammar, spelling, and tone of the text. After using this tool, the authors reviewed and edited the content as needed and take full responsibility for the content of the publication.

Conflicts of Interest: The authors declare that they have no known competing financial interests or personal relationships that could have appeared to influence the work reported in this paper.

References

1. Correia, J.R. 7—Pultrusion of advanced composites. In *Advanced Fiber-Reinforced Polymer(FRP) Composites for Structural Applications*, 2nd ed.; Bai, J., Ed.; Woodhead Publishing: London, UK, 2023; pp. 137–177.
2. Guades, E.; Aravinthan, T.; Islam, M.; Manalo, A. A review on the driving performance of FRP composite piles. *Compos. Struct.* **2012**, *94*, 1932–1942. [CrossRef]
3. Vedernikov, A.; Safonov, A.; Tucci, F.; Carlone, P.; Akhatov, I. Pultruded materials and structures: A review. *J. Compos. Mater.* **2020**, *54*, 4081–4117. [CrossRef]
4. Correia, J.R. Pultrusion of advanced fibre-reinforced polymer (FRP) composites. In *Advanced Fibre-Reinforced Polymer (FRP) Composites for Structural Applications*; Elsevier: Amsterdam, The Netherlands, 2013; pp. 207–251.
5. Singamsethi, S.; LaFave, J.; Hjelmstad, K. Fabrication and testing of cuff connections for GFRP box sections. *J. Compos. Constr.* **2005**, *9*, 536–544. [CrossRef]
6. Charoenphan, S.; Bank, L.C.; Plesha, M.E. Progressive tearing failure in pultruded composite material tubes. *Compos. Struct.* **2004**, *63*, 45–52. [CrossRef]
7. Boyd, S.; Dulieu-Barton, J.; Rumsey, L. Stress analysis of finger joints in pultruded GRP materials. *Int. J. Adhes. Adhes.* **2006**, *26*, 498–510. [CrossRef]
8. Rubino, F.; Nisticò, A.; Tucci, F.; Carlone, P. Marine application of fiber reinforced composites: A review. *J. Mar. Sci. Eng.* **2020**, *8*, 26. [CrossRef]
9. Ahn, N.; Lee, J.; Lee, K.; Jang, H.S. An experimental study on flexural behavior for a FRP composite girder. *Constr. Build. Mater.* **2014**, *50*, 13–21. [CrossRef]
10. Grammatikos, S.A.; Jones, R.G.; Evernden, M.; Correia, J.R. Thermal cycling effects on the durability of a pultruded GFRP material for off-shore civil engineering structures. *Compos. Struct.* **2016**, *153*, 297–310. [CrossRef]
11. Özkılıç, Y.O.; Madenci, E.; Safonov, A.; Gemi, L.; Yazman, Ş. Comprehensive evaluation of tensile properties, damage mechanisms, and predictive modeling of pultruded GFRP after elevated temperatures. *Compos. Part B Eng.* **2025**, *304*, 112657. [CrossRef]
12. Wu, C.; Ding, Y.; He, L.; Tam, L.-H. Web crippling of pultruded GFRP built-up sections. *Thin-Walled Struct.* **2023**, *185*, 110646. [CrossRef]
13. Gonilha, J.A.; Silvestre, N.; Correia, J.R.; Tita, V.; Martins, D. Novel progressive failure model for quasi-orthotropic pultruded FRP structures: Formulation and calibration of parameters (Part I). *Compos. Struct.* **2021**, *255*, 112974. [CrossRef]
14. Mosallam, A.S.; Abdelhamid, M.K.; Conway, J.H. Performance of pultruded FRP connections under static and dynamic loads. *J. Reinf. Plast. Compos.* **1994**, *13*, 386–407. [CrossRef]
15. Aksoylu, C.; Özkılıç, Y.O.; Madenci, E.; Safonov, A. Compressive behavior of pultruded GFRP boxes with concentric openings strengthened by different composite wrappings. *Polymers* **2022**, *14*, 4095. [CrossRef] [PubMed]
16. Zhang, L.; Li, Q.; Long, Y.; Cao, D.; Guo, K. Modelling of web-crippling behavior of pultruded GFRP I sections at elevated temperatures. *Polymers* **2022**, *14*, 5313. [CrossRef] [PubMed]
17. Jawaheri Zadeh, H.; Mejia, F.; Nanni, A. Strength reduction factor for flexural RC members strengthened with near-surface-mounted bars. *J. Compos. Constr.* **2013**, *17*, 614–625. [CrossRef]
18. Wang, C. Test on pultruded GFRP I-section under web crippling. *Compos. Part B Eng.* **2015**, *77*, 27–37. [CrossRef]
19. Wu, C.; Zhang, L.-T.; Tam, L.-h.; Yan, L.; He, L. Effect of bearing length on web crippling behavior of pultruded GFRP channel section. *Compos. Struct.* **2020**, *253*, 112810. [CrossRef]
20. Asghar, R.; Javed, M.F.; Ali, M.; Najeh, T.; Gamil, Y. Numerical and artificial intelligence based investigation on the development of design guidelines for pultruded GFRP RHS profiles subjected to web crippling. *Sci. Rep.* **2024**, *14*, 10135. [CrossRef] [PubMed]
21. Haloi, J.; Borsaikia, A.C.; Singh, K.D. New design equations for predicting web crippling capacity of pultruded GFRP profile. In *Proceedings of the Structures*; Elsevier: Amsterdam, The Netherlands, 2024; p. 106481.
22. Ye, Y.-Y.; Gonilha, J.; Silvestre, N.; Correia, J.R. Experimental study of web-crippling behavior of pultruded GFRP I-section profiles under localized one-flange loading. *Thin-Walled Struct.* **2025**, *209*, 112931. [CrossRef]
23. Ye, Y.-Y.; Gonilha, J.; Silvestre, N.; Correia, J.R. Web-crippling behavior of pultruded GFRP I-section beams under one-flange loading: Computational modelling and parametric study. *Compos. Part B Eng.* **2025**, *307*, 112915. [CrossRef]
24. Almeida-Fernandes, L.; Silvestre, N.; Correia, J.R. Fracture toughness-based models for web-crippling of pultruded GFRP profiles. *Compos. Part B Eng.* **2022**, *230*, 109541. [CrossRef]
25. Soumbourou, M.A.; Aksoylu, C.; Madenci, E.; Özkılıç, Y.O. Web Crippling of Pultruded GFRP Profiles: A Review of Experimental, Numerical, and Theoretical Analyses. *Polymers* **2025**, *17*, 2746. [CrossRef] [PubMed]
26. Wu, C.; Bai, Y. Web crippling behaviour of pultruded glass fibre reinforced polymer sections. *Compos. Struct.* **2014**, *108*, 789–800. [CrossRef]

27. Chen, Y.; Wang, C. Web crippling behavior of pultruded GFRP rectangular hollow sections. *Compos. Part B Eng.* **2015**, *77*, 112–121. [CrossRef]
28. Gand, A.; Mohammed, M.H.; Jarrouja, S. Performance of perforated FRP stub beams subject to static transverse actions. *Eng. Solid Mech.* **2020**, *8*, 105–118. [CrossRef]
29. Haloi, J.; Singh, K.D.; Borsaikia, A.C. Effect of web perforation on the performance of pultruded GFRP wide-flange section profile in web crippling under end-two-flange loading configuration. *Thin-Walled Struct.* **2022**, *175*, 109187. [CrossRef]
30. Haloi, J.; Borsaikia, A.C.; Singh, K.D. Web crippling behaviour of web perforated GFRP wide-flange sections subjected to interior-two-flange loading condition. *Thin-Walled Struct.* **2021**, *166*, 108072. [CrossRef]
31. Bai, Y.; Keller, T.; Correia, J.R.; Branco, F.A.; Ferreira, J.G. Fire protection systems for building floors made of pultruded GFRP profiles–Part 2: Modeling of thermomechanical responses. *Compos. Part B Eng.* **2010**, *41*, 630–636. [CrossRef]
32. Correia, J.R.; Bai, Y.; Keller, T. A review of the fire behaviour of pultruded GFRP structural profiles for civil engineering applications. *Compos. Struct.* **2015**, *127*, 267–287. [CrossRef]
33. Lin, S.-H.; Yu, W.-W.; Galambos, T.V.; Wang, E. Revised ASCE specification for the design of cold-formed stainless steel structural members. *Eng. Struct.* **2005**, *27*, 1365–1372. [CrossRef]
34. ASTM International. *ASTM D2584-11*; Standard Test Method for Ignition Loss of Cured Reinforced Resins. ASTM International: West Conshohocken, PA, USA, 2011.
35. Soumbourou, M.A.; Madenci, E.; Aksoylu, C.; Özkılıç, Y.O. Effect of the Hole Diameter Ratio (d/H) on the Web Crippling Capacity of Pultruded GFRP U-Channels Under Temperature and Loading Conditions. *Polymers* **2026**, *18*, 1002. [CrossRef] [PubMed]

Disclaimer/Publisher's Note: The statements, opinions and data contained in all publications are solely those of the individual author(s) and contributor(s) and not of MDPI and/or the editor(s). MDPI and/or the editor(s) disclaim responsibility for any injury to people or property resulting from any ideas, methods, instructions or products referred to in the content.